THE p-AAA ALGORITHM FOR DATA DRIVEN MODELING OF PARAMETRIC DYNAMICAL SYSTEMS*

ANDREA CARRACEDO RODRIGUEZ†, LINUS BALICKI‡, AND SERKAN GUGERCIN†§

Abstract. The AAA algorithm has become a popular tool for data-driven rational approximation of single variable functions, such as transfer functions of linear dynamical systems. In the setting of parametric dynamical systems appearing in many prominent applications, the underlying (transfer) function to be modeled is a multivariate function. With this in mind, we develop the AAA framework for approximating multivariate functions where the approximant is constructed in the multivariate barycentric form. The method is data-driven, in the sense that it does not require access to the full state-space model and requires only function evaluations. We discuss an extension to the case of matrix-valued functions, i.e., multi-input/multi-output dynamical systems, and provide a connection to the tangential interpolation theory. Several numerical examples illustrate the effectiveness of the proposed approach.

Key words. Rational approximation, parametric systems, dynamical systems, interpolation, least-squares, transfer functions

AMS subject classifications. 35B30,37M99, 41A20, 35B30, 65K99, 93A15, 93B15

1. Introduction. Many physical phenomena can be modeled as dynamical systems whose dynamics depend on one or several parameter values. These parameters might represent material properties, boundary conditions, system geometry, etc. As an example, consider an input-output system governed by a system of linear ordinary differential equations (can be viewed as a semi-discretized time-dependent PDE)

$$(1.1) \qquad \dot{\mathbf{x}}(t,p) = \mathbf{A}(p)\mathbf{x}(t,p) + \mathbf{b}f(t); \qquad y(t,p) = \mathbf{c}^\top \mathbf{x}(t,p),$$

where $p \in \mathcal{P} \subset \mathbb{R}$ represents the parametric variation in $\mathbf{A}(p) \in \mathbb{R}^{\rho \times \rho}$; $\mathbf{b}, \mathbf{c} \in \mathbb{R}^\rho$ are constant; $f(t) \in \mathbb{R}$ is the input (forcing term); $y(t,p) \in \mathbb{R}$ is the output (quantity of interest); and $\mathbf{x}(t,p) \in \mathbb{R}^\rho$ is the state (internal degrees of freedom). Assuming zero initial conditions, i.e., $\mathbf{x}(0) = \mathbf{0}$, the output $y(t,p)$ can be expressed using the convolution integral

$$(1.2) \qquad y(t,p) = \int_0^t \mathbf{c}^\top e^{(t-\tau)\mathbf{A}(p)} \mathbf{b} f(\tau) \ d\tau.$$

When the system dimension, ρ, is large, evaluating the quantity of interest $y(t,p)$ repeatedly for different parameter values becomes computationally demanding. One remedy to this problem is to find a surrogate model of much smaller dimension, i.e., a reduced dynamical system, so that re-evaluations of the system are significantly cheaper yet accurately captures $y(t,p)$. This is the goal of parametric model order

†Department of Mathematics, Virginia Tech, Blacksburg VA 24061, USA (crandrea@vt.edu).

‡Department of Mathematics, Virginia Tech, Blacksburg VA 24061, USA (balicki@vt.edu).

§Department of Mathematics and Computational Modeling and Data Analytics Division, Academy of Data Science, VA 24061, USA (gugercin@vt.edu).

reduction (PMoR). Projection-based PMoR methods have been successfully developed for systems with known internal description as in (1.1), i.e., the full-order operators $\mathbf{A}(p), \mathbf{b}$ and $\mathbf{c}$ are available; see, e.g., the recent survey papers and books [3, 7, 24, 42] for a detailed analysis of projection-based approaches to PMoR. However, in many cases the internal description of a system is not accessible and only input/output measurements are available. In our setting, for parametric dynamical systems such as (1.1), input/output measurements/data will correspond to the samples of *the transfer function* of (1.1), i.e., the samples of

$$(1.3) \qquad H(s,p) = \mathbf{c}^\top (s\mathbf{I} - \mathbf{A}(p))^{-1}\mathbf{b},$$

where $H(s,p)$ is the Laplace transform of the convolution kernel $h(t) = \mathbf{c}^\top e^{t\mathbf{A}(p)}\mathbf{b}$ in (1.2). Then, given the samples $\{H(s_i, p_j)\}$, our goal is to build a function that approximates this data in an appropriate measure. Even though our motivation comes from approximating parametric dynamical systems, similar approximation problems can also arise in modeling stationary PDEs, such as

$$u_{xx} + pu_{yy} + zu = f(x,y) \qquad \text{on} \qquad \Omega = [a,b] \times [c,d],$$

with appropriately defined initial and boundary conditions. A spatial discretization on Ω, yields

$$\mathbf{A}(p,z)\mathbf{u} = \mathbf{b}.$$

Then, the samples of the function $H(p,z) = \mathbf{A}(p,z)^{-1}\mathbf{b}$ can be used to build an approximation to the solution $u(x,y)$. We visit two such problems in Section 4.2. Assume, for the moment, that $\mathbf{A}(p)$ in (1.3) has an affine dependence on p, e.g., $\mathbf{A}(p) = \mathbf{A}_0 + p\mathbf{A}_1$ where $\mathbf{A}_0$ and $\mathbf{A}_1$ are constant matrices. Then, both $H(s,p)$ and $H(p,z)$ defined above are two-variable rational functions. That is, $H(s,p)$ (and similarly $H(p,z)$) can be expressed as a ratio of two-variable polynomials

$$H(s,p) = \frac{\sum_{i=0}^{k}\sum_{j=0}^{q}\tilde{\beta}_{ij}s^i p^j}{\sum_{i=0}^{k}\sum_{j=0}^{q}\tilde{\alpha}_{ij}s^i p^j}, \quad \tilde{\alpha}_{kq} \neq 0 \text{ or } \tilde{\beta}_{kq} \neq 0.$$

We refer to the tuple (k,q) as the *order* of $H(s,p)$. Further, we call $H(s,p)$ proper if $\tilde{\alpha}_{kq} \neq 0$ and $\tilde{\beta}_{kq} \neq 0$ and strictly proper if $\tilde{\alpha}_{kq} \neq 0$ and $\tilde{\beta}_{kq} = 0$. Even though in our approach below we do not require $H(s,p)$ to be a two-variable rational function in (s,p) (and thus, we do not require $\mathbf{A}(p)$ to have an affine dependence on p), this form motivates us to enforce a rational form in the approximant (as done in the classical rational approximation of single-variable functions).

Consider a scalar-valued function $H(s,p)$ of two variables and assume we only have access to its samples:

$$H(s_i, p_j) \in \mathbb{C} \qquad \text{for} \quad i = 1, \ldots, N \text{ and } j = 1, \ldots, M.$$

We assume that the sampling points are given and fixed, i.e., we are not investigating how to pick s_i and p_j. Our goal is, then, to find a two-variable rational function $\widetilde{H}(s,p)$ that is a *good* approximation of $H(s,p)$. We will specify later how we evaluate the quality of our approximation. Even though our motivation is that $H(s,p)$ represents the transfer function of a parametric dynamical system and we consider the variable s as frequency and p as the parameter, this is not restrictive and the approach can be considered as rational approximation of a multivariate function from its samples.

Additionally, since the proposed method will be purely based on function $(H(s, p))$ samples, there are no restrictions on the type of parameter dependence in the system to approximate. Moreover, the parameter dependence can appear in other system matrices besides $\mathbf{A}(p)$. In order to make the derivations clear, we first review, in Section 2, three of the existing algorithms for data-driven rational approximation in the single variable case: the Loewner framework [1,2], the vector fitting method [23], and the AAA algorithm [40]. We highlight the similarities and differences among these three approaches. In Section 3, we present the proposed method, the parametric AAA algorithm (p-AAA), for data-driven modeling of parametric dynamical systems, which extends the AAA algorithm [40] to the multivariate case. In Section 4 we show how to apply the proposed methodology to matrix-valued functions. Throughout Section 3 and Section 4, we use various examples to illustrate the success of the new methodology.

2. Revisiting the single variable problem. In this section, we briefly revisit three approaches for the single variable case that are pertinent to our work. The single variable function to be approximated can be considered as the transfer function of a non-parametric dynamical system, for example.

Consider a single variable function $H(s)$ and assume access to its samples

$$(2.1) \qquad h_i = H(s_i), \qquad s_i \in \mathbb{C}, \qquad \text{for} \quad i = 1, \ldots, N.$$

The three methods we discuss will build a rational function $\widetilde{H}(s)$ that approximates the given data by means of interpolation, least squares (LS) minimization, or a combination of both. A key component in each case is the barycentric representation [11] of a rational function, given by

$$(2.2) \qquad \widetilde{H}(s) = \frac{n(s)}{d(s)} = \frac{\displaystyle\sum_{i=1}^{k} \frac{\beta_i}{s - \sigma_i}}{\displaystyle\sum_{i=1}^{k} \frac{\alpha_i}{s - \sigma_i}},$$

where $\sigma_i \in \mathbb{C}$ are the support (interpolation) points, a subset of the sampling points $\{s_1, \ldots, s_N\}$, and $\beta_i, \alpha_i \in \mathbb{C}$ are the weights to be determined. The algorithms we describe will differ from each other in how they choose σ_i's, α_i's, and β_i's. Note that multiplying the numerator and denominator of $\widetilde{H}(s)$ by $\prod_{i=1}^{k}(s - \sigma_i)$ reveals that $\widetilde{H}(s)$ is indeed a rational function of degree $k - 1$.

2.1. The barycentric rational interpolant via Loewner matrices. Given the data (samples) in (2.1), the Loewner approach [1,2] builds a rational function $\widetilde{H}(s)$ in (2.2) such that $\widetilde{H}(s_i) = h_i$ for all $i = 1, \ldots, N$ (assuming a rational function of degree $k-1$ with this property exists). In this case we call $\widetilde{H}(s)$ a rational interpolant. Partition the sampling points and the corresponding function values:

$$\{s_1, \ldots, s_N\} = \{\sigma_1, \ldots, \sigma_k\} \cup \{\hat{\sigma}_1, \ldots, \hat{\sigma}_{N-k}\},$$
$$\{h_1, \ldots, h_N\} = \{g_1, \ldots, g_k\} \cup \{\hat{g}_1, \ldots, \hat{g}_{N-k}\}.$$

Interpolation at $\{\sigma_1, \sigma_2, \ldots, \sigma_k\}$ is attained by choosing

$$(2.3) \qquad \beta_i = g_i \alpha_i,$$

provided α_i's are nonzero. For interpolation at $\hat{\sigma}_i$, for $i = 1, 2, \ldots, N - k$, we set

$$H(\hat{\sigma}_i) - \widetilde{H}(\hat{\sigma}_i) = \hat{g}_i - \frac{n(\hat{\sigma}_i)}{d(\hat{\sigma}_i)} = \hat{g}_i - \sum_{j=1}^{k} \frac{g_j \alpha_j}{\hat{\sigma}_i - \sigma_j} \bigg/ \sum_{j=1}^{k} \frac{\alpha_j}{\hat{\sigma}_i - \sigma_j} = 0.$$

Multiplying out with the denominator, we obtain

$$\hat{g}_i \sum_{j=1}^{k} \frac{\alpha_j}{\hat{\sigma}_i - \sigma_j} - \sum_{j=1}^{k} \frac{g_j \alpha_j}{\hat{\sigma}_i - \sigma_j} = \sum_{j=1}^{k} \frac{(\hat{g}_i - g_j)\alpha_j}{\hat{\sigma}_i - \sigma_j} = \mathbf{e}_i^\top \mathbb{L} \mathbf{a} = 0,$$

where $\mathbf{e}_i \in \mathbb{R}^{N-k}$ denotes the ith unit vector, $\mathbf{a}^\top = [\alpha_1 \cdots \alpha_k]$, and $\mathbb{L} \in \mathbb{C}^{(N-k) \times k}$ is the Loewner matrix given by

$$(2.4) \qquad \mathbb{L} = \begin{bmatrix} \frac{\hat{g}_1 - g_1}{\hat{\sigma}_1 - \sigma_1} & \cdots & \frac{\hat{g}_1 - g_k}{\hat{\sigma}_1 - \sigma_k} \\ \vdots & \ddots & \vdots \\ \frac{\hat{g}_{N-k} - g_1}{\hat{\sigma}_{N-k} - \sigma_1} & \cdots & \frac{\hat{g}_{N-k} - g_k}{\hat{\sigma}_{N-k} - \sigma_k} \end{bmatrix}.$$

Hence to enforce interpolation at $\{\hat{\sigma}_1, \hat{\sigma}_2, \ldots, \hat{\sigma}_{N-k}\}$, the unknown coefficient vector $\mathbf{a}^\top = [\alpha_1 \cdots \alpha_k]$ is obtained by solving the linear system

$$(2.5) \qquad\qquad\qquad \mathbb{L} \mathbf{a} = \mathbf{0}$$

for $\mathbf{a} \neq \mathbf{0}$. In particular, $\mathbf{a}$ can be chosen as a singular vector associated with a zero singular value of $\mathbb{L}$ (assuming such a singular value exists). Here, we skip the details for the conditions on $\mathbb{L}$ and its null space to guarantee the existence and uniqueness of a degree $k - 1$ rational interpolant of the form (2.2) and refer the reader to [2, 3] for details. A simple case to consider is when $N = 2k - 1$. In this case, the Loewner matrix is $\mathbb{L} \in \mathbb{C}^{(k-1) \times k}$, with, at least, a one-dimensional nullspace. Considering the fact that a proper rational function of degree $k-1$ has $2k-1$ degrees of freedom (after normalization of the highest coefficient in the denominator), choosing $N = 2k - 1$ will yield a unique rational interpolant (under certain conditions [2, 3]). By introducing the notion of the shifted Loewner matrix, in [35] the Loewner approach has been extended to a state-formulation where the rational interpolant can be directly written in a state-space form, as in (1.3), without forming the barycentric form. However, for the parametric problems, the barycentric formulation is the key and we refer the reader to [3, 5, 35] and the references therein for the state-space based Loewner construction for modeling dynamical systems without parameter dependencies.

2.2. Vector fitting for rational least-squares approximation. Instead of constructing a rational interpolant, one can also consider building a rational approximant by fitting the data in a least-squares (LS) sense. Thus, given the samples (2.1), the goal is now to construct a rational function $\widetilde{H}(s)$ that solves the LS problem

$$\min_{\alpha_j, \beta_j} \sum_{i=1}^{N} |\widetilde{H}(s_i) - h_i|^2.$$

There are various approaches to solving rational LS approximation from measured data; see, e.g., [10, 13, 19, 23, 25, 26, 33, 37, 43] and the references therein. Due to its close connection to the barycentric form we consider here, we briefly review the vector fitting (VF) method of [23].

VF starts with a slightly revised version of $\widetilde{H}(s)$ with the form

$$(2.6) \qquad \widetilde{H}(s) = \frac{n(s)}{d(s)} = \frac{\displaystyle\sum_{i=1}^{k} \frac{\beta_i}{s - \sigma_i}}{1 + \displaystyle\sum_{i=1}^{k} \frac{\alpha_i}{s - \sigma_i}} + d_1 + se_1.$$

A fundamental difference from the interpolation framework of Section 2.1 is that $\{\sigma_i\}$ in (2.6) are *not* a subset of sampling points, are chosen independently, and in VF are updated at every step. The choice of $\{\sigma_i\}$ in (2.6) will be clarified later. The additional "1" in the denominator guarantees that the first term in $\widetilde{H}(s)$ is strictly proper. The term $d_1 + se_1$, if needed, allows polynomial growth around $s = \infty$, which could be necessary in approximating transfer functions corresponding to differential algebraic equations [9, 22, 36]. These details are not fundamental to the focus of this paper; therefore we skip those and assume $d_1 = e_1 = 0$. For details, we refer the reader to [21, 23].

Using (2.6), the LS error can be written as

$$\sum_{i=1}^{N} |\widetilde{H}(s_i) - h_i|^2 = \sum_{i=1}^{N} \frac{1}{|d(s_i)|^2} |n(s_i) - d(s_i)h_i|^2.$$

This is a nonlinear LS problem. Starting with an initial guess $d^{(0)}(s)$, Sanathanan and Koerner [43] converts this nonlinear LS problem into a sequence of weighted linear LS problems, which we will call the SK iteration:

$$\min_{n^{(j+1)}, d^{(j+1)}} \sum_{i=1}^{N} \left| \frac{n^{(j+1)}(s_i) - d^{(j+1)}(s_i)h_i}{d^{(j)}(s_i)} \right|^2, \quad j = 0, 1, 2, \ldots.$$

Note that the problem is now linear in the unknowns $n^{(j+1)}(s)$ and $d^{(j+1)}(s)$. The SK iteration uses the polynomial basis for $n(s)$ and $d(s)$. VF, instead, uses the barycentric form (2.6), which proves to be the crucial step since it allows updating $\{\sigma_i\}$ in each step. VF updates $\{\sigma_i\}$ as the zeros of the denominator $d^{(j)}(s)$ from the previous iteration, i.e., $d^{(j)}(\sigma_i^{(j+1)}) = 0$. This updating procedure for $\{\sigma_i\}$ and a proper rescaling result in a sequence of unweighted linear LS minimization problems of the form

$$\min_{\mathbf{a}^{(j+1)}} \left\| \mathcal{A}^{(j)} \mathbf{a}^{(j+1)} - \mathbf{h} \right\|_2,$$

where $\mathbf{h} = [h_1 \ \cdots \ h_N]^\top$, $\mathbf{a} = [\beta_1 \ \cdots \ \beta_k \ \alpha_1 \ \cdots \ \alpha_k]^\top$, and $\mathcal{A}^{(j)}$ is given by

$$\mathcal{A}^{(j)} = \begin{bmatrix} \frac{1}{s_1 - \sigma_1^{(j)}} & \frac{1}{s_1 - \sigma_2^{(j)}} & \cdots & \frac{1}{s_1 - \sigma_k^{(j)}} & \frac{-h_1}{s_1 - \sigma_1^{(j)}} & \frac{-h_1}{s_1 - \sigma_2^{(j)}} & \cdots & \frac{-h_1}{s_1 - \sigma_k^{(j)}} \\ \frac{1}{s_2 - \sigma_1^{(j)}} & \frac{1}{s_2 - \sigma_2^{(j)}} & \cdots & \frac{1}{s_2 - \sigma_k^{(j)}} & \frac{-h_2}{s_2 - \sigma_1^{(j)}} & \frac{-h_2}{s_2 - \sigma_2^{(j)}} & \cdots & \frac{-h_2}{s_2 - \sigma_k^{(j)}} \\ \vdots & \vdots & \vdots & \vdots & \vdots & \vdots & \vdots & \vdots \\ \frac{1}{s_N - \sigma_1^{(j)}} & \frac{1}{s_N - \sigma_2^{(j)}} & \cdots & \frac{1}{s_N - \sigma_k^{(j)}} & \frac{-h_N}{s_N - \sigma_1^{(j)}} & \frac{-h_N}{s_N - \sigma_2^{(j)}} & \cdots & \frac{-h_N}{s_N - \sigma_k^{(j)}} \end{bmatrix}.$$

Note that the Loewner matrix $\mathbb{L}$ appearing in the interpolation setting of Section 2.1 is now replaced with $\mathcal{A}^{(j)}$, which consists of a Cauchy and a diagonally-scaled Cauchy

matrix. Despite dependence on the barycentric form, there is a fundamental difference from the Loewner framework of Section 2.1: The coefficients $\{\alpha_i\}$ and $\{\beta_i\}$ in the barycentric form are chosen independently to minimize the LS error. This is in contrast to the Loewner setting where one sets $\beta_i = h_i \alpha_i$ to enforce interpolation. Moreover, the points $\{\sigma_i\}$ are updated at every step.

Convergence of VF is an open question. Even though one can construct examples where the iteration does not converge [32], its behavior in practice is more robust. When initial set $\{\sigma_i\}$ is chosen appropriately, the algorithm usually converges quickly. As VF converges, due to the updating scheme of $\{\sigma_i\}$, the denominator $d^{(k)}(s)$ converges to 1 and one obtains a pole-residue formulation for $\widetilde{H}(s)$. However, this is not needed. The algorithm can be terminated early with $\widetilde{H}(s)$ having the barycentric form as in (2.6).

2.3. The AAA algorithm. Given the samples $\{H(s_i)\}_{i=1}^N$, we have seen two frameworks for constructing $\widetilde{H}(s)$: the barycentric rational interpolation via Loewner matrices (Section 2.1) and the rational LS approximation via VF (Section 2.2). Both methods depend on the barycentric form and differ in how they choose the variables in this representation. The Adaptive Anderson-Antoulas (AAA) algorithm developed by Nakatsukasa et al. [40] is an iterative algorithm that elegantly integrates these two frameworks (interpolation and LS) combining their strengths, leading to a powerful framework for rational approximation.

As in Section 2.1, we partition the sampling points $\{s_i\}$ and the samples $\{h_i\}$ into two disjoint data sets:

(2.7)

$$\text{sampling points: } \{s_1, \ldots, s_N\} = \{\ \sigma_1, \ldots, \sigma_k\ \} \cup \{\ \hat{\sigma}_1, \ldots, \hat{\sigma}_{N-k}\ \} \overset{\text{def}}{=\!=} \{\ \boldsymbol{\sigma}\ \cup\ \hat{\boldsymbol{\sigma}}\ \},$$
$$\text{sampled values: } \{h_1, \ldots, h_N\} = \{\ g_1, \ldots, g_k\ \} \cup \{\ \hat{g}_1, \ldots, \hat{g}_{N-k}\ \} \overset{\text{def}}{=\!=} \{\ \mathbf{g}\ \cup\ \hat{\mathbf{g}}\ \}.$$

This partitioning will be clarified later. Assume the barycentric form for $\widetilde{H}(s)$ as in (2.2), which we repeat here:

$$(2.2) \qquad\qquad \widetilde{H}(s) = \frac{n(s)}{d(s)} = \sum_{i=1}^{k} \frac{\beta_i}{s - \sigma_i} \Bigg/ \sum_{i=1}^{k} \frac{\alpha_i}{s - \sigma_i}.$$

Now assume that, we want to enforce interpolation at the points $\boldsymbol{\sigma}$. Therefore, in (2.2) we set $\beta_i = g_i \alpha_i$ for $i = 1, 2, \ldots, k$, as we did in Section 2.1. However, as opposed to enforcing interpolation on $\hat{\boldsymbol{\sigma}}$ as well, AAA chooses the coefficients $\{\alpha_i\}$ to minimize the LS error over the remaining sampling points $\hat{\boldsymbol{\sigma}}$.

As in Section 2.2, the LS problem over the sampling points $\hat{\boldsymbol{\sigma}}$ is nonlinear due to dependence on the denominator $d(s)$. VF algorithm used the SK-iteration to convert this nonlinear LS problem to a sequence of linearized LS problems. AAA uses a different linearization. More precisely, for the point $\hat{\sigma}_i$, AAA uses the linearization

$$(2.8) \qquad H(\hat{\sigma}_i) - \widetilde{H}(\hat{\sigma}_i) = \hat{g}_i - \frac{n(\hat{\sigma}_i)}{d(\hat{\sigma}_i)} = \frac{1}{d(\hat{\sigma}_i)} \left(\hat{g}_i d(\hat{\sigma}_i) - n(\hat{\sigma}_i) \right)$$

$$(2.9) \qquad\qquad \rightsquigarrow \hat{g}_i d(\hat{\sigma}_i) - n(\hat{\sigma}_i) = \sum_{j=1}^{k} \frac{(\hat{g}_i - g_j)\alpha_j}{\hat{\sigma}_i - \sigma_j} = \mathbf{e}_i^\top \mathbb{L} \mathbf{a},$$

where $\mathbb{L}$ is the Loewner matrix defined as in (2.4) and $\mathbf{a} = [\alpha_1 \ \cdots \ \alpha_k]^\top$. This means we simply drop the term $1/d(\hat{\sigma}_i)$ in order to compute the coefficient vector $\mathbf{a}$ via the

linear LS problem (over $\hat{\boldsymbol{\sigma}}$), namely

$$(2.10) \qquad\qquad \min_{\|\mathbf{a}\|_2=1} \|\mathbb{L}\mathbf{a}\|_2\,.$$

Before elaborating on how AAA partitions the data set for interpolation and LS, we point out the difference between (2.5) and (2.10) in determining $\mathbf{a}$. In the interpolation case, assuming that there exists an underlying degree $k-1$ rational interpolant, the Loewner matrix has a null space and thus we solve $\mathbb{L}\mathbf{a} = 0$. On the other hand, in the case of linearized LS problem in AAA, such a rational interpolant does not exist (consider it as too many data points and not enough degrees of freedom), and one solves the minimization problem (2.10) by choosing $\mathbf{a}$ as the right singular vector corresponding to the smallest singular value of $\mathbb{L}$.

AAA iteratively partitions the data using a greedy search at each step. Let $\widetilde{H}(s)$ denote the AAA approximant at step k corresponding to the interpolation/LS data partitioning in (2.7). The next sampling point, σ_{k+1}, to be added to interpolation set $\boldsymbol{\sigma}$, is determined by finding $\hat{\sigma}_i$ for which the current error is maximum, i.e.,

$$\sigma_{k+1} = \arg\max_{i=1,\ldots,N-k} \left| H(\hat{\sigma}_i) - \widetilde{H}(\hat{\sigma}_i) \right|.$$

Then, the algorithm proceeds by updating the interpolation and LS data partition, setting $\beta_{k+1} = g_{k+1}\alpha_{k+1}$, and by solving (2.10) for the updated coefficient vector. AAA is terminated when either a pre-specified error tolerance or an order is achieved. We refer the reader to the original source [40] for details. We also note that a similar greedy search for computing interpolation points was proposed in [14,17] in projection-based interpolatory model reduction and in [31] in Loewner-based interpolatory modeling.

As AAA proceeds, a new column is added to $\mathbb{L}$ at every step. Therefore, assuming large number of data points N, the matrix $\mathbb{L}$ in AAA is tall and skinny, and thus generically does not have a null space. However, if $\mathbb{L}$ happens to have a nullspace after a certain iteration index, the AAA approximant will interpolate the full data set and coincide with the rational interpolant of Section 2.1, assuming a unique solution.

Remark 2.1. *Adding* $1/d(s)$ *as a weight.* It was pointed out in [40, §10] that one can introduce weighted norms in the LS problem in every step of AAA by scaling the rows of the Loewner matrix. Inspired by the SK iteration and VF, another type of weighting can be introduced by modifying the linearization step (2.9) in AAA as

$$H(\hat{\sigma}_i) - \widetilde{H}(\hat{\sigma}_i) = \frac{1}{d(\hat{\sigma}_i)}\left(\hat{g}_i d(\hat{\sigma}_i) - n(\hat{\sigma}_i)\right) \rightsquigarrow \frac{1}{d^-(\hat{\sigma}_i)}\left(\hat{g}_i d(\hat{\sigma}_i) - n(\hat{\sigma}_i)\right),$$

where $d^-(s)$ denotes the denominator of the AAA approximation from the previous step, thus keeping the error still linear in the variables $n(s)$ and $d(s)$ to be computed. Then, the coefficient vector $\mathbf{a}$ can be found by solving the weighted linear LS problem $\min_{\|\mathbf{a}\|_2=1} \|\Delta\mathbb{L}\mathbf{a}\|_2$, where Δ is a $k \times k$ diagonal matrix with the diagonal elements $\Delta_{ii} = 1/d^-(\hat{\sigma}_i)$. In our numerical experiments, this revised implementation applied to various examples did not result in a significant advantage. The only improvement we observed, and only in some cases, was a reduction by one unit in the order of the rational approximation corresponding to the same error tolerance. Due to these numerical observations, we do not investigate this further here or in the multivariate case below. Note that this weighting strategy by $1/d(s)$ focuses on adding weighting during AAA. In two recent works [18,41] in the setting of rational minimax approximation, AAA is followed by the Lawson algorithm [30], an iteratively weighed LS

iteration, yielding the AAA-Lawson method. The weighting in AAA-Lawson appears in the Lawson step, not in AAA.

The AAA algorithm has proved very successful and has been employed in many applications including nonlinear eigenvalue problems [34], rational minimax approximation [18], and rational approximations over disconnected domains [40]. Our goal, in the following sections, is to extend AAA to approximating parametric (dynamical) systems from their samples.

3. p-AAA: AAA for parametric dynamical systems. In this section, we introduce the parametric AAA (p-AAA) algorithm, which extends AAA to multi-variable problems appearing in the modeling of (the transfer function of) parametric dynamical systems. We start with the two-variable case first and illustrate its performance on various examples. Then, we briefly discuss how p-AAA can be applied to functions with more than two variables followed by an application to such an example. In this section, to simplify the initial discussion, we only focus on scalar-valued functions. The p-AAA for matrix valued functions is discussed in Section 4.

3.1. p-AAA for the two-parameter case. We consider the problem of rational approximation of a multivariate function $H(s, p)$ from data. We assume only access to the samples of $H(s, p)$, i.e., we have

$$(3.1) \qquad h_{ij} = H(s_i, p_j) \in \mathbb{C} \qquad \text{for} \quad i = 1, \ldots, N \text{ and } j = 1, \ldots, M.$$

Analogously to the single-variable case, we express the rational approximant $\widetilde{H}(s, p)$ in its *two-variable* barycentric form

$$(3.2) \qquad \widetilde{H}(s, p) = \frac{n(s, p)}{d(s, p)} = \sum_{i=1}^{k} \sum_{j=1}^{q} \frac{\beta_{ij}}{(s - \sigma_i)(p - \pi_j)} \bigg/ \sum_{i=1}^{k} \sum_{j=1}^{q} \frac{\alpha_{ij}}{(s - \sigma_i)(p - \pi_j)},$$

where $\{\sigma_i\}$ and $\{\pi_j\}$ are to-be-determined points, subsets of $\{s_i\}$ and $\{p_j\}$, respectively; and β_{ij} and α_{ij} are scalar coefficients to be chosen based on the interpolation and LS conditions to be enforced on the data (3.1). Similar to the single variable case multiplying $n(s, p)$ and $d(s, p)$ by $\prod_{i=1}^{k} \prod_{j=1}^{q} (s - \sigma_i)(p - \pi_j)$ reveals that $\widetilde{H}(s, p)$ is a two-variable rational function of order $(k - 1, q - 1)$. The number of points, k, in the variable-s and q in the variable-p will be automatically determined by the algorithm. We start by partitioning the data (3.1):

$$
\begin{aligned}
&\{s_1, \ldots, s_N\} = \{\sigma_1, \ldots, \sigma_k\} \cup \{\hat{\sigma}_1, \ldots, \hat{\sigma}_{N-k}\} \overset{\text{def}}{=\!=} \{\boldsymbol{\sigma} \ \cup \ \hat{\boldsymbol{\sigma}}\}, \\
&\{p_1, \ldots, p_M\} = \{\pi_1, \ldots, \pi_q\} \cup \{\hat{\pi}_1, \ldots, \hat{\pi}_{M-q}\} \overset{\text{def}}{=\!=} \{\boldsymbol{\pi} \ \cup \ \hat{\boldsymbol{\pi}}\}, \text{ and}
\end{aligned}
$$

$$(3.3) \qquad \left[\begin{array}{c|c} [H(\sigma_i, \pi_j)] & [H(\sigma_i, \hat{\pi}_j)] \\ \hline [H(\hat{\sigma}_i, \pi_j)] & [H(\hat{\sigma}_i, \hat{\pi}_j)] \end{array} \right] \overset{\text{def}}{=\!=} \left[\begin{array}{c|c} \mathbf{D}_{\boldsymbol{\sigma}\boldsymbol{\pi}} & \mathbf{D}_{\boldsymbol{\sigma}\hat{\boldsymbol{\pi}}} \\ \hline \mathbf{D}_{\hat{\boldsymbol{\sigma}}\boldsymbol{\pi}} & \mathbf{D}_{\hat{\boldsymbol{\sigma}}\hat{\boldsymbol{\pi}}} \end{array} \right],$$

where $[H(\sigma_i, \pi_j)] = \mathbf{D}_{\boldsymbol{\sigma}\boldsymbol{\pi}}$ denotes the $k \times q$ matrix whose (i, j)th entry is $H(\sigma_i, \pi_j)$; and similarly for other quantities such as $[H(\sigma_i, \hat{\pi}_j)] = \mathbf{D}_{\boldsymbol{\sigma}\hat{\boldsymbol{\pi}}}$. We use $\mathbf{D}_{\boldsymbol{\sigma}\boldsymbol{\pi}}$ to denote the sampled data corresponding to the sampling points $(\boldsymbol{\sigma}, \boldsymbol{\pi})$ (and similarly for other samples) as opposed to $\mathbf{H}_{\boldsymbol{\sigma}\boldsymbol{\pi}}$ since $H(s, p)$ will be used in Section 4 to denote matrix-valued (transfer) functions. How data is partitioned as in (3.3) will be clarified later.

Interpolation of the sampled data $\mathbf{D}_{\boldsymbol{\sigma\pi}}$. In accordance with the partitioning of the data in (3.3), first we enforce interpolation at $(\boldsymbol{\sigma}, \boldsymbol{\pi})$, i.e., on the (1,1) block $\mathbf{D}_{\boldsymbol{\sigma\pi}}$, of the sampled data. This is achieved by setting, in (3.2),

$$\beta_{ij} = H(\sigma_i, \pi_j)\alpha_{ij}, \tag{3.4}$$

assuming $\alpha_{ij} \neq 0$. This follows from the fact that, as in the single variable case, the barycentric form $\widetilde{H}(s, p)$ in (3.2) has a removable singularity at (σ_i, π_j) with $\widetilde{H}(\sigma_i, \pi_j) = \beta_{ij}/\alpha_{ij}$ [4], and the choice (3.4) leads to interpolation of the data in $\mathbf{D}_{\boldsymbol{\sigma\pi}}$. This determines β_{ij}. What remains to fully specify $\widetilde{H}(s, p)$ is the choice of α_{ij}.

LS fit for the uninterpolated data. The rational approximant $\widetilde{H}(s, p)$ in (3.2) with the choice (3.4), interpolates the data $\mathbf{D}_{\boldsymbol{\sigma\pi}}$. Next, we show how to chose α_{ij} so that $\widetilde{H}(s, p)$ minimizes the LS error in the remaining sampled data set in $\mathbf{D}_{\boldsymbol{\sigma\hat{\pi}}}$, $\mathbf{D}_{\boldsymbol{\hat{\sigma}\pi}}$, and $\mathbf{D}_{\boldsymbol{\hat{\sigma}\hat{\pi}}}$, i.e., to minimize

$$\|\boldsymbol{\varepsilon}\|_2 = \left\| \begin{bmatrix} \boldsymbol{\varepsilon}_1 \\ \boldsymbol{\varepsilon}_2 \\ \boldsymbol{\varepsilon}_3 \end{bmatrix} \right\|_2 \stackrel{\text{def}}{=} \left\| \begin{bmatrix} \mathsf{vec}(\mathbf{D}_{\boldsymbol{\sigma\hat{\pi}}}) \\ \mathsf{vec}(\mathbf{D}_{\boldsymbol{\hat{\sigma}\pi}}) \\ \mathsf{vec}(\mathbf{D}_{\boldsymbol{\hat{\sigma}\hat{\pi}}}) \end{bmatrix} - \begin{bmatrix} \mathsf{vec}(\widetilde{H}(\boldsymbol{\sigma}, \boldsymbol{\hat{\pi}})) \\ \mathsf{vec}(\widetilde{H}(\boldsymbol{\hat{\sigma}}, \boldsymbol{\pi})) \\ \mathsf{vec}(\widetilde{H}(\boldsymbol{\hat{\sigma}}, \boldsymbol{\hat{\pi}})) \end{bmatrix} \right\|_2 . \tag{3.5}$$

As in the single variable case, the resulting LS problem is nonlinear and we will linearize it similarly. To illustrate this more clearly, we rewrite the error for a sample $(\hat{\sigma}, \hat{\pi})$ in the set $(\boldsymbol{\hat{\sigma}}, \boldsymbol{\hat{\pi}})$ corresponding to a component in $\boldsymbol{\varepsilon}_3$ in (3.5) as

$$
\begin{aligned}
H(\hat{\sigma}, \hat{\pi}) - \widetilde{H}(\hat{\sigma}, \hat{\pi}) &= H(\hat{\sigma}, \hat{\pi}) - \frac{n(\hat{\sigma}, \hat{\pi})}{d(\hat{\sigma}, \hat{\pi})} \\
&= \frac{1}{d(\hat{\sigma}, \hat{\pi})} \left(H(\hat{\sigma}, \hat{\pi}) d(\hat{\sigma}, \hat{\pi}) - n(\hat{\sigma}, \hat{\pi}) \right) \\
&\rightsquigarrow H(\hat{\sigma}, \hat{\pi}) d(\hat{\sigma}, \hat{\pi}) - n(\hat{\sigma}, \hat{\pi}) \quad \text{(linearization)} \\
&= H(\hat{\sigma}, \hat{\pi}) \sum_{i=1}^{k} \sum_{j=1}^{q} \frac{\alpha_{ij}}{(\hat{\sigma} - \sigma_i)(\hat{\pi} - \pi_j)} - \sum_{i=1}^{k} \sum_{j=1}^{q} \frac{H(\sigma_i, \pi_j)\alpha_{ij}}{(\hat{\sigma} - \sigma_i)(\hat{\pi} - \pi_j)} \\
&= \sum_{i=1}^{k} \sum_{j=1}^{q} \frac{(H(\hat{\sigma}, \hat{\pi}) - H(\sigma_i, \pi_j))\alpha_{ij}}{(\hat{\sigma} - \sigma_i)(\hat{\pi} - \pi_j)} \\
&= \mathbf{e}_{\hat{\sigma}\hat{\pi}}^{\top} \mathbb{L}_{\hat{\sigma}\hat{\pi}} \, \mathbf{a},
\end{aligned}
$$

where

$$\mathbf{a}^{\top} = [\alpha_{11} \cdots \alpha_{1q} \mid \cdots \mid \alpha_{k1} \cdots \alpha_{kq}] \in \mathbb{C}^{kq}, \tag{3.6}$$

$\mathbb{L}_{\hat{\boldsymbol{\sigma}}\hat{\boldsymbol{\pi}}} \in \mathbb{C}^{(N-k)(M-q)\times(kq)}$ is the 2D Loewner matrix[1] defined by

(3.7)

$$
\mathbb{L}_{\hat{\boldsymbol{\sigma}}\hat{\boldsymbol{\pi}}} =
\left[
\begin{array}{ccc|c}
\frac{H(\hat{\sigma}_1,\hat{\pi}_1)-H(\sigma_1,\pi_1)}{(\hat{\sigma}_1-\sigma_1)(\hat{\pi}_1-\pi_1)} & \cdots & \frac{H(\hat{\sigma}_1,\hat{\pi}_1)-H(\sigma_1,\pi_q)}{(\hat{\sigma}_1-\sigma_1)(\hat{\pi}_1-\pi_q)} & \cdots \\
& \vdots & & \\
\frac{H(\hat{\sigma}_{N-k},\hat{\pi}_{M-q})-H(\sigma_1,\pi_1)}{(\hat{\sigma}_{N-k}-\sigma_1)(\hat{\pi}_{M-q}-\pi_1)} & \cdots & \frac{H(\hat{\sigma}_{N-k},\hat{\pi}_{M-q})-H(\sigma_1,\pi_q)}{(\hat{\sigma}_{N-k}-\sigma_1)(\hat{\pi}_{M-q}-\pi_q)} & \cdots
\end{array}
\right.
$$

$$
\left.
\begin{array}{c|ccc}
\cdots & \frac{H(\hat{\sigma}_1,\hat{\pi}_1)-H(\sigma_k,\pi_1)}{(\hat{\sigma}_1-\sigma_k)(\hat{\pi}_1-\pi_1)} & \cdots & \frac{H(\hat{\sigma}_1,\hat{\pi}_1)-H(\sigma_k,\pi_q)}{(\hat{\sigma}_1-\sigma_k)(\hat{\pi}_1-\pi_q)} \\
& & \vdots & \\
\cdots & \frac{H(\hat{\sigma}_{N-k},\hat{\pi}_{M-q})-H(\sigma_k,\pi_1)}{(\hat{\sigma}_{N-k}-\sigma_k)(\hat{\pi}_{M-q}-\pi_1)} & \cdots & \frac{H(\hat{\sigma}_{N-k},\hat{\pi}_{M-q})-H(\sigma_k,\pi_q)}{(\hat{\sigma}_{N-k}-\sigma_k)(\hat{\pi}_{M-q}-\pi_q)}
\end{array}
\right],
$$

and $\mathbf{e}_{\hat{\sigma}\hat{\pi}} \in \mathbb{R}^{(N-k)(M-q)}$ is the unit vector with 1 in the entry corresponding to the sample $(\hat{\sigma},\hat{\pi})$. Therefore, the linearized error $\boldsymbol{\varepsilon}_3$ is given by $\mathbb{L}_{\hat{\boldsymbol{\sigma}}\hat{\boldsymbol{\pi}}} \mathbf{a}$. Note that $\mathbb{L}_{\hat{\boldsymbol{\sigma}}\hat{\boldsymbol{\pi}}}$ has a nested structure that takes the differences of all combinations of samples into consideration. The entries are explicitly given by:

$$
\mathbb{L}_{\hat{\boldsymbol{\sigma}}\hat{\boldsymbol{\pi}}}(\hat{j}+(M-q)(\hat{\imath}-1), j+q(i-1)) = \frac{H(\hat{\sigma}_{\hat{\imath}},\hat{\pi}_{\hat{\jmath}}) - H(\sigma_i,\pi_j)}{(\hat{\sigma}_{\hat{\imath}}-\sigma_i)(\hat{\pi}_{\hat{\jmath}}-\pi_j)},
$$

for $\hat{\jmath} = 1,\ldots,M-q$, $\hat{\imath} = 1,\ldots,N-k$, $j = 1,\ldots,q$, and $i = 1,\ldots,k$.

The procedure follows similarly for the other blocks in (3.5). First note that

$$
\widetilde{H}(\sigma_i,\hat{\pi}_\ell) = \sum_{j=1}^{q} \frac{\beta_{ij}}{\hat{\pi}_\ell - \pi_j} \Bigg/ \sum_{j=1}^{q} \frac{\alpha_{ij}}{\hat{\pi}_\ell - \pi_j} \ .
$$

This expression together with the definition of β_{ij} in (3.4) allow us to write the error corresponding to a sample $(\sigma_i,\hat{\pi}_\ell)$ in ε_1 in (3.5) as

$$
H(\sigma_i,\hat{\pi}_\ell) - \widetilde{H}(\sigma_i,\hat{\pi}_\ell) = \left(\sum_{j=1}^{q} \frac{H(\sigma_i,\hat{\pi}_\ell) - H(\sigma_i,\pi_j)}{\hat{\pi}_\ell - \pi_j} \alpha_{ij} \right) \Bigg/ \sum_{j=1}^{q} \frac{\alpha_{ij}}{\hat{\pi}_\ell - \pi_j}
$$

$$
\rightsquigarrow \sum_{j=1}^{q} \frac{H(\sigma_i,\hat{\pi}_\ell) - H(\sigma_i,\pi_j)}{\hat{\pi}_\ell - \pi_j} \alpha_{ij} \quad \text{(linearization)}
$$

$$
= \mathbf{e}_\ell^\top \mathbb{L}_{\sigma_i} \mathbf{a}_i,
$$

where $\mathbf{a}_i^\top = [\alpha_{i1}\cdots\alpha_{iq}] \in \mathbb{C}^q$ is the ith row block of $\mathbf{a}$, $\mathbf{e}_\ell \in \mathbb{C}^{M-q}$ is the ℓth unit vector, and $\mathbb{L}_{\sigma_i} \in \mathbb{C}^{(M-q)\times q}$ is the regular (1D) Loewner matrix corresponding to the data in the ith row of $[\mathbf{D}_{\boldsymbol{\sigma}\boldsymbol{\pi}}\ \mathbf{D}_{\boldsymbol{\sigma}\hat{\boldsymbol{\pi}}}]$, i.e.,

(3.8) $(\mathbb{L}_{\sigma_i})_{\ell,j} = \dfrac{H(\sigma_i,\hat{\pi}_\ell) - H(\sigma_i,\pi_j)}{\hat{\pi}_\ell - \pi_j}$ for $\ell = 1,2,\ldots,M-q$ and $j = 1,2,\ldots,q$.

Similar to [27], define

(3.9) $\mathbb{L}_{\boldsymbol{\sigma}\hat{\boldsymbol{\pi}}} = \mathsf{diag}(\mathbb{L}_{\sigma_1},\ldots,\mathbb{L}_{\sigma_k}) \in \mathbb{C}^{(k(M-q))\times(kq)}$.

---

[1]Similar to the single-variable case, the Loewner matrices appearing in p-AAA here also appear in the parametric Loewner framework [4, 27] where one aims to interpolate the full data set. We revisit these connections in Remark 3.2.

Then, the linearized error corresponding to $\boldsymbol{\varepsilon}_1$ in (3.5) is given by $\mathbb{L}_{\boldsymbol{\sigma}\hat{\boldsymbol{\pi}}}\mathbf{a}$. Similarly, we can linearize and rewrite the error for the $\boldsymbol{\varepsilon}_2$-block in (3.5) as $\mathbb{L}_{\hat{\boldsymbol{\sigma}}\boldsymbol{\pi}}\mathbf{a}$ where $\mathbb{L}_{\hat{\boldsymbol{\sigma}}\boldsymbol{\pi}}$ is an assembly of all 1D Loewner matrices $\mathbb{L}_{\pi_j}$ corresponding to the data in each column of $\begin{bmatrix} \mathbf{D}_{\boldsymbol{\sigma}\boldsymbol{\pi}} \\ \mathbf{D}_{\hat{\boldsymbol{\sigma}}\boldsymbol{\pi}} \end{bmatrix}$. Putting all three together, after linearization, minimizing the LS error (3.5) in p-AAA becomes

$$(3.10) \qquad \min_{\|\mathbf{a}\|_2=1} \|\mathbb{L}_2\mathbf{a}\|_2 \quad \text{where} \quad \mathbb{L}_2 = \begin{bmatrix} \mathbb{L}_{\boldsymbol{\sigma}\hat{\boldsymbol{\pi}}}^\top & \mathbb{L}_{\hat{\boldsymbol{\sigma}}\boldsymbol{\pi}}^\top & \mathbb{L}_{\hat{\boldsymbol{\sigma}}\hat{\boldsymbol{\pi}}}^\top \end{bmatrix}^\top \in \mathbb{C}^{(MN-kq)\times kq}.$$

We summarize this analysis in a corollary.

COROLLARY 3.1. *Consider the data* (3.3) *and let the corresponding barycentric rational approximant* $\widetilde{H}(s,p)$ *have the form in* (3.2).
(a) If (3.4) *holds, then*

$$\widetilde{H}(\sigma_i,\pi_j) = H(\sigma_i,\pi_j), \quad i=1,\dots,k, \ j=1,\dots,q.$$

(b) Assume (3.4) *holds. Choose the indices* α_{ij} *using*

$$(3.11) \quad [\alpha_{11}\cdots\alpha_{1q} \mid \cdots \mid \alpha_{k1}\cdots\alpha_{kq}] = \boldsymbol{a}^\star \quad \text{where} \quad \boldsymbol{a}^\star = \arg\min_{\|\boldsymbol{a}\|_2=1}\|\mathbb{L}_2\boldsymbol{a}\|_2,$$

where $\mathbb{L}_2$ *is as defined in* (3.10), *with* $\mathbb{L}_{\hat{\boldsymbol{\sigma}}\hat{\boldsymbol{\pi}}}$ *is as given by* (3.7), $\mathbb{L}_{\boldsymbol{\sigma}\hat{\boldsymbol{\pi}}}$ *by* (3.9) *and* (3.8), *and* $\mathbb{L}_{\hat{\boldsymbol{\sigma}}\boldsymbol{\pi}}$ *is defined as*

$$\mathbb{L}_{\hat{\boldsymbol{\sigma}}\boldsymbol{\pi}} = \begin{bmatrix} \mathbb{L}_{\pi_1}\boldsymbol{e}_1 & & & \\ & \ddots & & \cdots \\ & & \mathbb{L}_{\pi_q}\boldsymbol{e}_1 & \end{bmatrix} \begin{array}{|c} \mathbb{L}_{\pi_1}\boldsymbol{e}_k \\ \ddots \\ \mathbb{L}_{\pi_q}\boldsymbol{e}_k \end{array} \Big] \in \mathbb{C}^{(q(N-k))\times(kq)},$$

where

$$(3.12) \quad \mathbb{L}_{\pi_j}(\hat{\imath},i) = \frac{H(\hat{\sigma}_{\hat{\imath}},\pi_j) - H(\sigma_i,\pi_j)}{\hat{\sigma}_{\hat{\imath}} - \sigma_i}, \quad \hat{\imath}=1,\dots,N-k, \ i=1,\dots,k,$$

and $\boldsymbol{e}_i \in \mathbb{C}^k$ *is the* ith *unit vector. Then, the two-variable barycentric approximant minimizes the linearized LS error*

$$\widetilde{H} = \arg\min_{\hat{H}=n/d} \sum_{i,j} |H(s_i,p_j)d(s_i,p_j) - n(s_i,p_j)|^2$$

for the samples (s_i,p_j) *corresponding to the error* $\boldsymbol{\varepsilon}$ *in* (3.5), *i.e., for the data in* $\{\boldsymbol{D}_{\boldsymbol{\sigma}\hat{\boldsymbol{\pi}}}, \boldsymbol{D}_{\hat{\boldsymbol{\sigma}}\boldsymbol{\pi}}, \boldsymbol{D}_{\hat{\boldsymbol{\sigma}}\hat{\boldsymbol{\pi}}}\}$.

Choosing the interpolated vs LS-fitted data. The last component of p-AAA is determining how to choose the data to be interpolated and the data to be fitted in the LS sense. Let $\widetilde{H}(s,p)$ in (3.2) be the current p-AAA approximant corresponding to the interpolation/LS partitioning in (3.3). Note that the order of the current approximation is $(k-1,q-1)$ and these orders need not be equal. Then, we select the next frequency-parameter tuple (σ_{k+1},π_{q+1}) by means of the greedy search

$$(3.13) \qquad (s_{\hat{\imath}},p_{\hat{\jmath}}) = \arg\max_{(i,j)} |H(s_i,p_j) - \widetilde{H}(s_i,p_j)|.$$

We do not simply set $(\sigma_{k+1}, \pi_{q+1}) = (s_{\hat{i}}, p_{\hat{j}})$ since one of the entries might already be in the previous interpolation data. In other words, $s_{\hat{i}}$ might already be in the set $\boldsymbol{\sigma}$ or $p_{\hat{j}}$ might already be in the set $\boldsymbol{\pi}$ in (3.3). We note that this cannot occur for $s_{\hat{i}}$ and $p_{\hat{j}}$ simultaneously since we impose interpolation on the selected tuples. In other words, if the tuple $(s_{\hat{i}}, p_{\hat{j}})$ was already in the interpolated data, we would have had $H(s_{\hat{i}}, p_{\hat{j}}) - \widetilde{H}(s_{\hat{i}}, p_{\hat{j}}) = 0$, which means the whole data set is interpolated. If the point $p_{\hat{j}}$ is already in the set $\boldsymbol{\pi}$ in (3.3), then the order in the variable-p remains unchanged as $q - 1$ and the set $\boldsymbol{\pi}$ is not altered. On the other hand, the point $s_{\hat{i}}$ is added to set $\boldsymbol{\sigma}$ in (3.3) and the order in the variable-s is increased to k. Conversely, $p_{\hat{j}}$ is added to $\boldsymbol{\pi}$ and $s_{\hat{i}}$ is not added to $\boldsymbol{\sigma}$ if the point $s_{\hat{i}}$ is already in the set $\boldsymbol{\sigma}$. This allows updating the orders in each variable independently, giving the algorithm flexibility to make the decision automatically. Once the data partitioning (3.3) (and the orders) are updated, p-AAA computes the new coefficients β_{ij} as in (3.4), and then solves the LS problem (3.10) for the updated coefficient vector $\mathbf{a}$. The process is repeated until either a pre-specified error tolerance or desired orders in (s, p) are achieved. We give a brief sketch of p-AAA in Algorithm 3.1. We use the notation $[x_{ij}]$ to denote a matrix whose (i, j)th entry is x_{ij}.

Algorithm 3.1 p-AAA

1: Given $\{s_i\}$, $\{p_j\}$, and $\{h_{ij}\} = \{H(s_i, p_j)\}$
2: Initialize: $k = 0$ and $q = 0$
3: Define $\widetilde{H} = average(h_{ij})$ and set error $\leftarrow \frac{\|[h_{ij}] - [\widetilde{H}]\|_\infty}{\|[h_{ij}]\|_\infty}$
4: **while** error $>$ desired tolerance **do**
5:     Select $(s_{\hat{i}}, p_{\hat{j}})$ by the greedy search (3.13)
6:     Update the data partitioning (3.3):
7:     **if** $s_{\hat{i}}$ was not selected at a previous iteration **then**
8:         $k \leftarrow k + 1$
9:         $\sigma_k \leftarrow s_{\hat{i}}$
10:     **end if**
11:     **if** $p_{\hat{j}}$ was not selected at a previous iteration **then**
12:         $q \leftarrow q + 1$
13:         $\pi_q \leftarrow p_{\hat{j}}$
14:     **end if**
15:     Build $\mathbb{L}_2$ as in (3.10)
16:     Solve $\min \|\mathbb{L}_2 \mathbf{a}\|_2$ s.t. $\|\mathbf{a}\|_2 = 1$
17:     Use $\mathbf{a}$ to update the rational approximant $\widetilde{H}(s, p)$ with (3.2)–(3.4)
18:     error $\leftarrow \frac{\|[h_{ij}] - [\widetilde{H}(s_i, p_j)]\|_\infty}{\|[h_{ij}]\|_\infty}$
19: **end while**
20: **return** $\widetilde{H}$

Remark 3.2. *Parametric Loewner framework.* As in the single-variable case discussed in Section 2.1, one can choose to construct an approximation that interpolates the full-data (3.1) as done in [4, 27]. In this case, based on the ranks of Loewner matrices, the orders k and q are chosen large enough so that, unlike in p-AAA, the matrix $\mathbb{L}_2$ has a null space and thus one chooses the coefficient vector $\mathbf{a}$ by solving the linear system $\mathbb{L}_2 \mathbf{a} = \mathbf{0}$. Therefore, the parametric Loewner framework [4, 27] interpolates the full data in contrast to p-AAA, which greedily chooses a subset of data to interpolate and performs LS fit on the rest. When the orders k and q are

not chosen *large enough*, the parametric Loewner framework no longer yields an interpolant, and instead a Loewner *approximant* is obtained. For details we refer the reader to [3–5, 27]. Even though this situation is more similar to the case of p-AAA, the major difference lies in the fact that p-AAA is an iterative algorithm and chooses the interpolation data with a greedy search while performing LS fit on the rest. In other words, p-AAA decides the data-partitioning (3.3) automatically using a greedy search with an appropriately defined criterion. On the other hand, the parametric Loewner framework is a one-step algorithm and how to partition the data is not yet fully understood. Even though there have been recent efforts in this direction for the single-variable case [16, 28, 29], this is still an open question, especially in the multivariate case. It will be worthwhile to investigate how the final data partitioning from p-AAA affects the parametric Loewner construction and whether it improves the conditioning-issues, appearing, at times, in the (one-step) Loewner framework.

Remark 3.3. *Real state-space realization.* When working with dynamical systems, it is often desirable to have access to system matrices that constitute a state-space form similar to the one presented in (1.1). The system matrices are typically real-valued, a desirable property to retain in the rational approximant as well. As outlined in Appendix A, real state-space representations based on two-variable barycentric forms can be computed if all samples in the p and s-variables are real valued [27]. In the dynamical system setting the parameter samples are generically real valued whereas the frequency are usually complex-valued. In order to ensure realness in the complex case, the frequencies need to be sampled in complex-conjugate pairs. This means that if $s_i \in \mathbb{C}$ is sampled, we also sample $\bar{s}_i$. Then, if $s_{\hat{i}}$ in Step 7 of Algorithm 3.1 is a complex frequency, we also add $\bar{s}_{\hat{i}}$ to the interpolation data set and Line 8 of Algorithm 3.1 becomes $k \leftarrow k + 2$. We follow this approach in the examples discussed in Subsections 3.2.2 and 3.3.1. Algorithmic details are explained in Appendix A.

Remark 3.4. An important property of the single-variable AAA algorithm is that either one obtains an approximant with a desired accuracy or an interpolant of minimal order. Although p-AAA has similar properties, the interpolant may not be of minimal order. (This is illustrated in the numerical example of Section 3.2.1.) We emphasize that this is only an issue for small synthetic examples as we consider in Section 3.2.1 where the underlying model is a low-order multi-parameter rational function to begin with. In most practical situations of interest (indeed for all the other examples we have considered), we obtain an approximant; not an exact recovery. A post-processing routine which ensures minimal order of interpolants (in case they occur) is presented in Appendix B.

3.2. Numerical Examples. Next, we illustrate the performance of p-AAA on three numerical examples.

3.2.1. Synthetic Transfer Function. We use a simple model from [27], which is a low-order rational function in two variables. Consider

$$H(s,p) = \frac{1}{1 + 25(s+p)^2} + \frac{0.5}{1 + 25(s-0.5)^2} + \frac{0.1}{p + 25}.$$

We sample this transfer function at $H(s_i, p_j)$ for $N = M = 21$ frequency and parameter points linearly spaced in $s_i \in [-1, 1]$ and $p_j \in [0, 1]$. This is a rational function with order $(4, 3)$. p-AAA terminates after 7 iterations. Table 1 shows the greedy search selection at each iteration step. Additionally, quantities related to the post-processing step presented in Appendix B are shown. Note that the p-AAA approximation $\tilde{H}$

iter.	greedy selection	σ_k	π_q	(k, q)	$\dim \ker \mathbb{L}_2$
1	$(0, 0)$	0	0	(1,1)	0
2	$(-1, 0)$	-1		(2,1)	0
3	$(0.1, 0)$	0.1		(3,1)	0
4	$(0, 1)$		1	(3,2)	0
5	$(-1, 0.6)$		0.6	(3,3)	0
6	$(-0.6, 0.1)$	-0.6	0.1	(4,4)	0
7	$(0.6, 0.55)$	0.6	0.55	(5,5)	2
post-processing as in Appendix B				(5,4)	1

TABLE 1

Example 3.2.1 p-AAA samples selected at each iteration

(without the post-processing) would have been of order $(k - 1, q - 1) = (4, 4)$, as opposed to $(4, 3)$ of the original model. This is due to the greedy search selecting frequencies and parameters to interpolate as tuples hence allowing for repetition. In Table 1 we see exactly how this happened for this example. During iterations 2 and 3, no parameters are added for interpolation while during iterations 4 and 5, no frequencies are added for interpolation. Upon convergence, for this simple example where the underlying function is a low-order rational function itself, p-AAA exactly recovers it. In other words, after step 7, all the data is interpolated. This shows another flexibility of p-AAA. If the underlying order is low enough, the LS component is automatically converted to a full interpolation, thus, in this special example, giving the same approximant as the parametric Loewner approach [27].

We present in Figure 1 the evolution of the p-AAA approximant at various iterations: first, third, and last (seventh). As Figure 1 shows that, upon convergence, the proposed algorithm captures the full model exactly.
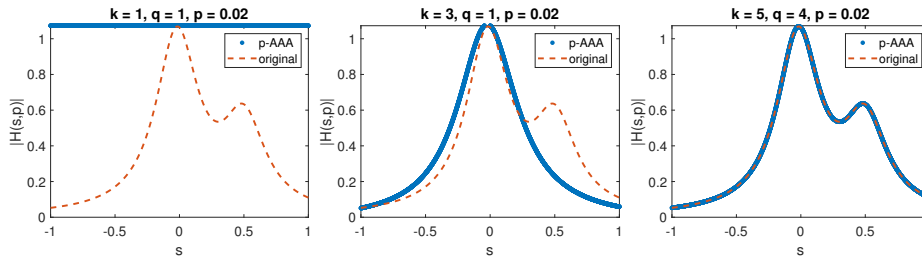

FIG. 1. *Example 3.2.1: p-AAA approximation at various iterations*

3.2.2. A beam model. In this example, we consider the finite element model of a one-dimensional Euler-Bernoulli beam with a string attached near its left boundary and an input force applied at its right boundary, as shown in Figure 2. As for the output $y(t)$, we measure the displacement at the right boundary where the forcing is applied. We take the stiffness coefficient of the spring as the parameter and obtain the parametric dynamical system

$$\mathbf{M}\ddot{\mathbf{x}}(t, p) + \mathbf{G}\dot{\mathbf{x}}(t, p) + \mathbf{K}(p)\mathbf{x}(t, p) = \mathbf{b}f(t), \quad y(t, p) = \mathbf{c}^\top \mathbf{x}(t, p),$$
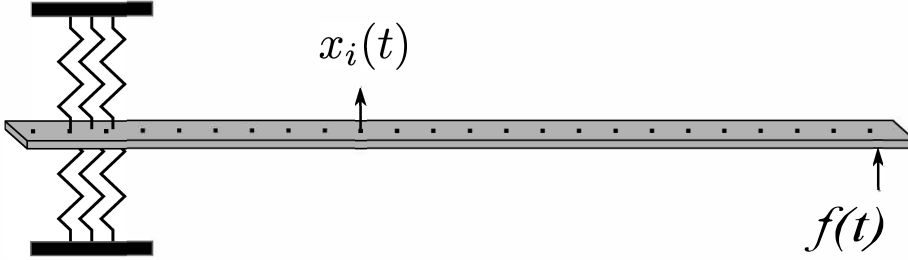
FIG. 2. *Example 3.2.2: Visualization of an Euler-Bernoulli beam*
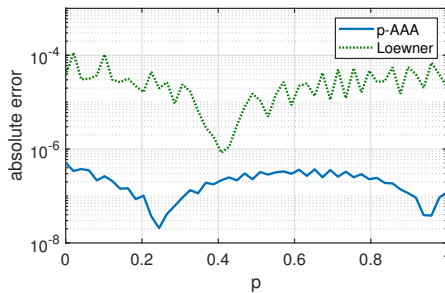
FIG. 3. *Example 3.2.2:* **p-AAA** *approximation for various parameter values and Loewner approximation with the same order as* **p-AAA**.

with the corresponding transfer function

$$H(s, p) = \mathbf{c}^\top (s^2 \mathbf{M} + s\mathbf{G} + \mathbf{K}(p))^{-1} \mathbf{b},$$

where $\mathbf{M}$ and $\mathbf{G}$ are, respectively, the mass and damping matrices; $\mathbf{K}(p)$ is the parametric stiffness matrix; and $\mathbf{b}$ and $\mathbf{c}$ are, respectively, the input-to-state and the state-to-output mappings. We measure the transfer function at $H(s_i, p_j)$ for $N = 3000$ frequency points $\{s_i\}$ in the interval $[0, 2\pi \times 10^3]\imath$ where $\imath^2 = -1$ and for $M = 3$ parameter values $p_1 = 0.2$, $p_2 = 0.4$, and $p_3 = 1$. p-AAA yields an approximant with orders $(k, q) = (19, 2)$. Out of three parameter samples, p-AAA chooses $p_2 = 0.4$ and $p_3 = 1$ for interpolation. Using the same parameter and frequency samples, we also construct the parametric Loewner approximant [27]. Figure 4 shows the amplitude frequency responses of the original transfer function $H(s, p)$, and the p-AAA and parametric Loewner approximants for various parameter values, including values that did not enter into p-AAA or parametric Loewner construction ($p = 0.8$ and $p = 15$ in Figure 4). Both p-AAA and parametric Loewner yield highly accurate approximations, capturing the peaks in the frequency response accurately. To check the accuracy of the p-AAA and parametric Loewner approximants further, we perform an exhaustive search over the parameter domain by computing, for 50 linearly spaced $\hat{p} \in [0, 1]$, the worst-case frequency domain error, i.e., $\max_s | H(s, \hat{p}) - \widetilde{H}(s, \hat{p}) |$ where $s = \imath\omega$ with $\omega \in [0, 2\pi \times 10^3]$. We use 3000 ω samples to approximate the maximum error. The results in Figure 3 show that p-AAA is accurate throughout the full parameter domain and, for this example, outperforms the parametric Loewner approach.
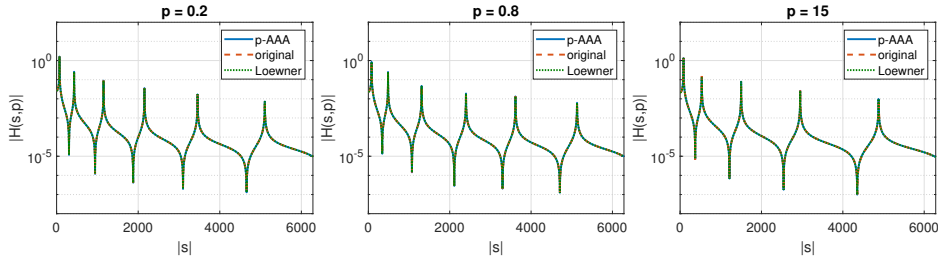
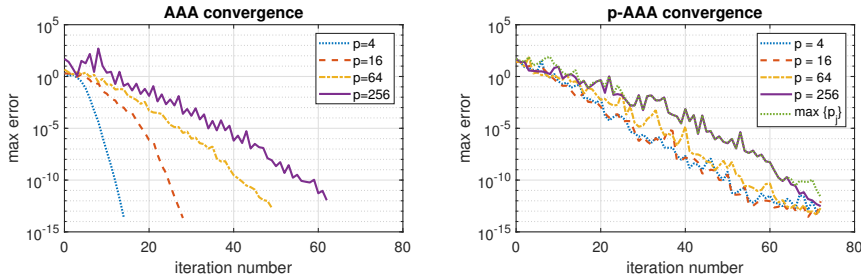Fig. 4. *Example 3.2.2: p-AAA and Loewner approximations in the s-interval sampled.*

Fig. 5. *Example 3.2.3: Convergence of AAA compared with p-AAA.*

3.2.3. p-AAA convergence behaviour. In this section we demonstrate the convergence behavior of p-AAA using a general multivariate function, not related to dynamical systems. To do so we consider an example from [40] where the goal is to approximate the function $\tan(ps)$. We take $N = 1000$ equispaced sample points on the unit circle for the s variable and a set of 9 parameter samples $\{2^0, 2^1, \ldots, 2^8\}$. For a comparison, (the single variable) AAA has been executed for $p = 4, 16, 64, 256$ We note that AAA has been run for every p value separately. This is in contrast to p-AAA where p-AAA is run only once and the resulting parametric approximant can be used for any given parameter value. For both algorithms a relative error tolerance of 10^{-13} was used. The parametric rational approximant computed by p-AAA after 73 iterations is of order $(70, 8)$. In Figure 5 we illustrate the differences in the convergence behaviour of AAA and p-AAA implementations. The left-hand side plot in Figure 5 depicts maximum errors over all sampled s-variables during individual (single variable) AAA runs for the four parameter choices of $p = 4, 16, 64, 256$. The right-hand side plot in Figure 5 shows the maximum error with respect to all sampled s and p values, denoted by the legend "$\max\{p_j\}$" (corresponding to the error in Line 18 of Algorithm 3.1 used as a convergence criterion). During the p-AAA implementation, we also monitor the maximum s-errors corresponding to the $p = 4, 16, 64, 256$ samples. We emphasize that these errors values for specific p values are not part of the p-AAA stopping criterion. p-AAA only monitors the maximum error over all the s and p samples. These are computed here only for comparison purposes. Figure 5 illustrates that AAA convergence speed varies with the magnitude of p (faster convergence for the smaller p values) whereas in p-AAA errors decrease uniformly across the parameter set mainly dictated by the hardest case. Overall, p-AAA needs more iterations to converge than AAA for a given fixed parameter. However, as mentioned above, we

need to run the parametric algorithm only once in order to obtain a single approximating function for all four rational functions computed by individual AAA runs. This example demonstrates that p-AAA is a viable choice in the general multivariate rational approximation setting and by no means restricted to the approximation of system dynamics in the frequency domain.

3.3. p-AAA for more than two parameters. The p-AAA algorithm extends analogously to the cases with more than two variables. To keep the discussion concise, we briefly highlight the three-variable case.

In this case, the underlying (transfer) function to approximate, $H(s, p, z)$, is a function of the three variables, s, p, and z, and we assume access to the sampling data

$$(3.14) \quad h_{ij\ell} = H(s_i, p_j, z_\ell) \in \mathbb{C} \quad \text{for} \quad i = 1, \dots, N, \quad j = 1, \dots, M, \quad \text{and} \quad \ell = 1, \dots, O.$$

The approximant $\widetilde{H}(s, p, z)$ is represented in the barycentric form given by
(3.15)
$$\widetilde{H}(s, p, z) = \sum_{i=1}^{k} \sum_{j=1}^{q} \sum_{\ell=1}^{o} \frac{\beta_{ij\ell}}{(s - \sigma_i)(p - \pi_j)(z - \zeta_\ell)} \Big/ \sum_{i=1}^{k} \sum_{j=1}^{q} \sum_{\ell=1}^{o} \frac{\alpha_{ij\ell}}{(s - \sigma_i)(p - \pi_j)(z - \zeta_\ell)},$$

where $\{\sigma_i\}$, $\{\pi_j\}$, and $\{\zeta_\ell\}$ are to-be-determined sampling points, subsets of $\{s_i\}$, $\{p_j\}$, and $\{z_\ell\}$, respectively. As in the two-variable case, $\beta_{ij\ell}$ will be chosen to enforce interpolation in a subset of the data and $\alpha_{ij\ell}$ to minimize a linearized LS error in the remaining data.

In accordance with the data (3.14) and the approximant $\widetilde{H}(s, p, z)$, partition the sampling points:

$$[s_1, \dots, s_N] = [\sigma_1, \dots, \sigma_k] \cup [\hat{\sigma}_1, \dots, \hat{\sigma}_{N-k}] = [\boldsymbol{\sigma} \mid \hat{\boldsymbol{\sigma}}],$$
(3.16)
$$[p_1, \dots, p_M] = [\pi_1, \dots, \pi_q] \cup [\hat{\pi}_1, \dots, \hat{\pi}_{M-q}] = [\boldsymbol{\pi} \mid \hat{\boldsymbol{\pi}}], \quad \text{and}$$
$$[z_1, \dots, z_O] = [\zeta_1, \dots, \zeta_o] \cup [\hat{\zeta}_1, \dots, \hat{\zeta}_{O-o}] = [\boldsymbol{\zeta} \mid \hat{\boldsymbol{\zeta}}].$$

Then, p-AAA imposes interpolation on the samples $\{\boldsymbol{\sigma}, \boldsymbol{\pi}, \boldsymbol{\zeta}\}$ by setting

$$(3.17) \quad \beta_{ij\ell} = H(\sigma_i, \pi_j, \zeta_\ell)\alpha_{ij\ell}, \quad \text{for } i = 1, \dots, k, \; j = 1, \dots, q, \; \text{and}, \; \ell = 1, \dots, o.$$

Based on the partitioning (3.16), consider the data as a three-dimensional tensor. We enforce interpolation in the $(1, 1, 1)$ block of this tensor with the choice in (3.17). Then, p-AAA minimizes the linearized LS error in the rest of the data by choosing the remaining coefficients $\mathbf{a} = [\alpha_{111} \cdots \alpha_{11o} | \alpha_{121} \cdots \alpha_{12o} | \cdots | \alpha_{kq1} \cdots \alpha_{kqo}]^\top$ via the linear LS problem $\min_{\|\mathbf{a}\|_2 = 1} \|\mathbb{L}_3 \mathbf{a}\|_2$ where $\mathbb{L}_3$ is the 3D Loewner matrix, which plays the same role the 2D Loewner matrix $\mathbb{L}_2$ played in Section 3.1. Partioning of the data in (3.16) is automatically established via the greedy search in every step.

Generalization to functions of more than three variables follows analogously. We skip those details due to cumbersome notation. However the potential computational difficulties with the increasing number of variables is worth elaborating. Assume that at the current step of p-AAA, we have the approximant $\widetilde{H}(s, p, z)$ as in (3.15). Given the sampling data in (3.14), this will result in $\mathbb{L}_3$ having $NMO - kqo$ rows and kqo columns. Therefore computing the coefficient vector $\mathbf{a}$ becomes more expensive as the number of variables (and the orders in each variable) increase. For functions with many variables, if the coefficient matrix becomes prohibitively large to compute $\mathbf{a}$ via direct methods, one might revert to well-established iterative approaches. For the numerical examples we considered in this paper, these computational complications did not arise and direct methods were readily available to apply.

3.3.1. Parameterized Gyroscope Model. In this section, we use p-AAA to approximate the dynamics of a microelectromechanical system (MEMS) gyroscope. The benchmark is available through [44] and further information regarding the background as well as the the operation principle of the MEMS gyroscope are discussed in [39]. Similar to the example in Section 3.2.2, the time-domain description of the system is given by the second-order model

$$\mathbf{M}(p)\ddot{\mathbf{x}}(t, p, z) + \mathbf{G}(p, z)\dot{\mathbf{x}}(t, p, z) + \mathbf{K}(p)\mathbf{x}(t, p, z) = \mathbf{b}, \quad y(t, p, z) = \mathbf{c}^{\top}\mathbf{x}(t, p, z),$$

where the mass matrix $\mathbf{M}(p) = \mathbf{M}_1 + p\mathbf{M}_2$, damping matrix $\mathbf{G}(p, z) = z(\mathbf{G}_1 + p\mathbf{G}_2)$ and stiffness matrix $\mathbf{K}(p) = \mathbf{K}_1 + \frac{1}{p}\mathbf{K}_2 + p\mathbf{K}_3$ are defined with respect to the structural parameter p and the rotation velocity z. We use p-AAA to approximate the corresponding three-variable transfer function

$$H(s, p, z) = \mathbf{c}^{\top}(s^2\mathbf{M}(p) + s\mathbf{G}(p, z) + \mathbf{K}(p))^{-1}\mathbf{b},$$

in the operating frequency range of the device, which corresponds to $s \in [2\pi \times 0.025, 2\pi \times 0.25]\imath$. For this example we chose to sample 100 linearly spaced frequencies in the aforementioned interval as well as 10 linearly spaced points in $[1, 2]$ for the p parameter and 10 logarithmically spaced points in $[10^{-7}, 10^{-5}]$ for the z parameter. After 33 iterations of p-AAA we obtain an approximant with order $(k, q, o) = (62, 7, 9)$ and a maximum relative error of 8.9×10^{-4} throughout the sampled domain. Figure 6 depicts the transfer function $H(s, p, z)$ for multiple unsampled parameter values. The frequency response drastically varies for different parameters, thus making it a function which is difficult to approximate. This may partially be due to the non-linear parameter dependence of the matrix $\mathbf{K}(p)$. In spite of these difficulties, p-AAA is able to produce good approximations for most parameters in the intervals of interest.
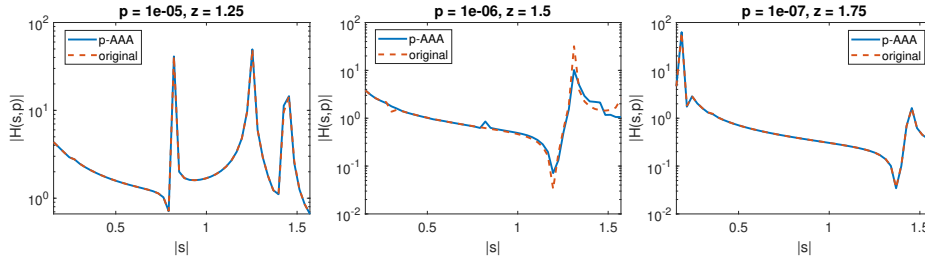
FIG. 6. *Example 3.3.1: p-AAA approximation of gyroscope model for various parameter combinations.*

4. p-AAA for matrix-valued functions. So far, we have considered approximating scalar-valued functions $H(s, p)$. In this section, we discuss p-AAA for approximating matrix-valued functions instead. This is a common situation, especially arising in the case of dynamical systems where the underlying system has multiple-inputs and multiple-outputs (MIMO), leading to matrix-valued transfer functions. Motivated by our interest in approximating dynamical systems, we will call the resulting method MIMO p-AAA. To keep the notation concise, we will present the discussion for the two-variable case. But as in Section 3.3, the results similarly extend to higher-dimensional parametric problems.

Let $\mathbf{H}(s, p)$ denote the underlying MIMO (transfer) function with n_{in} inputs and n_{out} outputs. Therefore, for the sampling points $\{s_i\}_{i=1}^{N}$ and $\{p_j\}_{j=1}^{M}$, we have access to the matrix-valued sampling data:

$$(4.1) \qquad \mathbf{H}_{ij} = \mathbf{H}(s_i, p_j) \in \mathbb{C}^{n_{in} \times n_{out}} \quad \text{for } i = 1, \ldots, N \quad \text{and} \quad j = 1, \ldots, M.$$

From the data (4.1), the goal is to construct a high-fidelity, matrix-valued approximant $\widetilde{\mathbf{H}}(s, p)$ to $\mathbf{H}(s, p)$.

4.1. Transformation to scalar-valued data. For the single-variable (non-parametric case), one solution to handle the matrix-valued data in AAA is to vectorize every sample and replace the scalar data forming the Loewner matrix $\mathbb{L}$ with the vectorized data. This is closely related to the approach proposed in Lietaert *et al.* [34] for using AAA in nonlinear eigenvalue problems. It is also analogous to how VF handles MIMO problems. One potential disadvantage of this approach is that, in the case of large number of inputs and outputs, the resulting Loewner matrix will have large dimensions, leading to a computational expensive LS step. Exploiting the fact that only certain rows and columns of the underlying Loewner matrix change in every step, [34] partially alleviates this computational complexity. However, for the parametric problems we consider here, dimension growth due to vectorization is more prominent and we will adopt another approach introduced by [15] for the nonparametric case, which transforms the MIMO data to a scalar one, and apply AAA to this scalar-valued data. We will extend this approach to parametric problems and establish what it means, for MIMO p-AAA, in terms of interpolation and the LS minimization.

As in the scalar case, assume the partitioning of the data in (4.1) as follows:

$$
(4.2) \quad
\begin{aligned}
\{s_1, \ldots, s_N\} &= \{\sigma_1, \ldots, \sigma_k\} \cup \{\hat{\sigma}_1, \ldots, \hat{\sigma}_{N-k}\} \overset{\text{def}}{=\!=\!=} \{\boldsymbol{\sigma} \; \cup \; \hat{\boldsymbol{\sigma}}\}, \\
\{p_1, \ldots, p_M\} &= \{\pi_1, \ldots, \pi_q\} \cup \{\hat{\pi}_1, \ldots, \hat{\pi}_{M-q}\} \overset{\text{def}}{=\!=\!=} \{\boldsymbol{\pi} \; \cup \; \hat{\boldsymbol{\pi}}\}, \text{ and} \\
\begin{bmatrix} [\mathbf{H}(\sigma_i, \pi_j)] & [\mathbf{H}(\sigma_i, \hat{\pi}_j)] \\ [\mathbf{H}(\hat{\sigma}_i, \pi_j)] & [\mathbf{H}(\hat{\sigma}_i, \hat{\pi}_j)] \end{bmatrix} &\overset{\text{def}}{=\!=\!=} \begin{bmatrix} \mathbf{D}_{\boldsymbol{\sigma}\boldsymbol{\pi}} & \mathbf{D}_{\boldsymbol{\sigma}\hat{\boldsymbol{\pi}}} \\ \mathbf{D}_{\hat{\boldsymbol{\sigma}}\boldsymbol{\pi}} & \mathbf{D}_{\hat{\boldsymbol{\sigma}}\hat{\boldsymbol{\pi}}} \end{bmatrix}.
\end{aligned}
$$

This partitioning will be determined by applying p-AAA to a scalar data set described below. In accordance with this partitioning, we want to construct $\widetilde{\mathbf{H}}(s, p)$ with the matrix-valued barycentric form

$$(4.3) \qquad \widetilde{\mathbf{H}}(s, p) = \frac{\mathbf{N}(s, p)}{d(s, p)} = \sum_{i=1}^{k} \sum_{j=1}^{q} \frac{\mathbf{B}_{ij}}{(s - \sigma_i)(p - \pi_j)} \bigg/ \sum_{i=1}^{k} \sum_{j=1}^{q} \frac{\tilde{\alpha}_{ij}}{(s - \sigma_i)(p - \pi_j)},$$

where $\mathbf{B}_{ij} \in \mathbb{C}^{n_{in} \times n_{out}}$ and $\tilde{\alpha}_{ij} \in \mathbb{C}$ are to be determined.

Motivated by [15] for the nonparametric case, we convert the matrix-valued data (4.1) to the scalar one by picking two random unit vectors $\mathbf{w} \in \mathbb{C}^{n_{out}}$ and $\mathbf{v} \in \mathbb{C}^{n_{in}}$, and computing

$$(4.4) \qquad h_{ij} = \mathbf{w}^{\top} \mathbf{H}(s_i, p_j) \mathbf{v} \quad \text{for } i = 1, \ldots, N \quad \text{and} \quad j = 1, \ldots, M.$$

We apply p-AAA to the scalar data (4.4) to obtain the scalar-valued rational approximation, as in (3.2):

$$(4.5) \quad \widetilde{H}(s, p) = \frac{n(s, p)}{d(s, p)} = \sum_{i=1}^{k} \sum_{j=1}^{q} \frac{\left(\mathbf{w}^{\top} \mathbf{H}(\sigma_i, \pi_j) \mathbf{v}\right) \alpha_{ij}}{(s - \sigma_i)(p - \pi_j)} \bigg/ \sum_{i=1}^{k} \sum_{j=1}^{q} \frac{\alpha_{ij}}{(s - \sigma_i)(p - \pi_j)}.$$

Note that $\beta_{ij} = \mathbf{w}^\top \mathbf{H}(\sigma_i, \pi_j) \mathbf{v} \alpha_{ij}$. Then, the final matrix-valued approximant $\widetilde{\mathbf{H}}(s, p)$ is obtained by setting $\tilde{\alpha}_{ij} = \alpha_{ij}$ and $\mathbf{B}_{ij} = \alpha_{ij} \mathbf{H}(\sigma_i, \pi_j)$ in (4.3), resulting in

$$(4.6) \qquad \widetilde{\mathbf{H}}(s, p) = \frac{\mathbf{N}(s, p)}{d(s, p)} = \sum_{i=1}^{k} \sum_{j=1}^{q} \frac{\mathbf{H}_{ij} \alpha_{ij}}{(s - \sigma_i)(p - \pi_j)} \bigg/ \sum_{i=1}^{k} \sum_{j=1}^{q} \frac{\alpha_{ij}}{(s - \sigma_i)(p - \pi_j)}.$$

As in the scalar p-AAA case, by construction, our choice of $\mathbf{B}_{ij}$ guarantees interpolation of the data for the samples $\{\boldsymbol{\sigma}, \boldsymbol{\pi}\}$ in (4.2). However, the (linearized) LS minimization is different. We summarize these results next.

Proposition 4.1. Given the sampling data (4.1), let $\widetilde{\mathbf{H}}(s, p)$ in (4.6) be the resulting approximant obtained via MIMO p-AAA with $\alpha_{ij} \neq 0$ and with the corresponding data partitioning (4.2). Then, $\widetilde{\mathbf{H}}(s, p)$ interpolates the data in $\mathbf{D}_{\boldsymbol{\sigma}\boldsymbol{\pi}}$ corresponding to the samples $\{\boldsymbol{\sigma}, \boldsymbol{\pi}\}$, i.e.,

$$(4.7) \qquad \widetilde{\mathbf{H}}(\sigma_i, \pi_j) = \mathbf{H}(\sigma_i, \pi_j) \ \text{ for } \ i = 1, \ldots, k \ \text{ and } \ j = 1, \ldots, q.$$

Furthermore, $\widetilde{\mathbf{H}}(s, p)$ minimizes an input/output weighted linearized LS measure, namely

$$(4.8) \qquad \widehat{\mathbf{H}} = \underset{\hat{\mathbf{H}} = \mathbf{N}/d}{\arg\min} \sum_{i,j} \left| \mathbf{w}^\top \big(\mathbf{H}(s_i, p_j) d(s_i, p_j) - \mathbf{N}(s_i, p_j) \big) \mathbf{v} \right|^2$$

for the data in $\{\mathbf{D}_{\boldsymbol{\sigma}\hat{\boldsymbol{\pi}}}, \mathbf{D}_{\hat{\boldsymbol{\sigma}}\boldsymbol{\pi}}, \mathbf{D}_{\hat{\boldsymbol{\sigma}}\hat{\boldsymbol{\pi}}}\}$, not selected by the greedy search, i.e., corresponding to the sampling pairs $(s_i, p_j) \in \{\{\hat{\boldsymbol{\sigma}}, \boldsymbol{\pi}\} \cup \{\boldsymbol{\sigma}, \hat{\boldsymbol{\pi}}\} \cup \{\hat{\boldsymbol{\sigma}}, \hat{\boldsymbol{\pi}}\}\}$.

Proof. Interpolation property (4.7) follows analogous to the scalar case, by observing that for $\alpha_{ij} \neq 0$, $\widetilde{\mathbf{H}}(s, p)$ has a removable pole at each (σ_i, π_j) with

$$\widetilde{\mathbf{H}}(\sigma_i, \pi_j) = \frac{\mathbf{B}_{ij}}{\alpha_{ij}}.$$

Then, the choice $\mathbf{B}_{ij} = \alpha_{ij} \mathbf{H}_{ij}$ proves (4.7).

To prove (4.8), first recall that $\widetilde{H}(s, p)$ in (4.4) is obtained by applying (scalar-valued) p-AAA to the data (4.4). Therefore, by Corollary 3.1,

$$(4.9) \qquad \widetilde{H} = \underset{\hat{H} = d/n}{\arg\min} \sum_{i,j} \left| \mathbf{w}^\top \mathbf{H}(s_i, p_j) \mathbf{v} d(s_i, p_j) - n(s_i, p_j) \right|^2.$$

Using (4.5) and (4.6), we have $\widetilde{H}(s, p) = \frac{n(s,p)}{d(s,p)} = \mathbf{w}^\top \widetilde{\mathbf{H}}(s, p) \mathbf{v} = \frac{\mathbf{w}^\top \mathbf{N}(s,p) \mathbf{v}}{d(s,p)}$. Therefore,

$$\mathbf{w}^\top \mathbf{H}(s_i, p_j) \mathbf{v} d(s_i, p_j) - n(s_i, p_j) = \mathbf{w}^\top \big(\mathbf{H}(s_i, p_j) d(s_i, p_j) - \mathbf{N}(s_i, p_j) \big) \mathbf{v}.$$

Inserting this last equality into (4.9) proves (4.8). $\qquad \qquad \square$

Remark 4.2. Proposition 4.1 states that for MIMO p-AAA, interpolation holds analogously to the scalar case. However, the LS minimization differs from the scalar case in that what is minimized is a weighted LS measure. More precisely, in terms of the LS aspect of MIMO p-AAA, the linearization is performed on the weighted error $\mathbf{w}^\top (\mathbf{H}(s, p) - \widetilde{\mathbf{H}}(s, p)) \mathbf{v}$.

Remark 4.3. When the internal description of the underlying (transfer) function is available, as in (1.1) and (1.3), projection-based approaches are commonly

used to construct interpolatory parametric approximants [3, 6, 8]. In this setting, for MIMO systems, one usually does not enforce full matrix interpolation. Instead, interpolation is enforced along selected *tangential directions*. In other words, one picks vectors $\mathbf{w}_i \in \mathbb{C}^{n_{out}}$ and $\mathbf{v}_i \in \mathbb{C}^{n_{in}}$ such that $\mathbf{H}(\sigma_i, \pi_j)\mathbf{v}_i = \widetilde{\mathbf{H}}(\sigma_i, \pi_j)\mathbf{v}_i$ and/or $\mathbf{w}_i^\top \mathbf{H}(\sigma_i, \pi_j) = \mathbf{w}_i^\top \widetilde{\mathbf{H}}(\sigma_i, \pi_j)$. This is called tangential interpolation. Tangential vectors usually vary with the sampling points. At this point, it is not clear, at least to us, how to achieve tangential interpolation using the barycentric form (4.3). However, inspired by this concept, instead of choosing two fixed vectors $\mathbf{w}$ and $\mathbf{v}$, one could pick different vectors $\mathbf{w}_i$, and $\mathbf{v}_i$ for each sample σ_i, for example and apply MIMO p-AAA to the data $\mathbf{w}_i^\top \mathbf{H}_{ij}\mathbf{v}_i$ to build the MIMO approximation (4.6) as above. The resulting model $\widetilde{\mathbf{H}}(s, p)$ would still interpolate the data $\mathbf{D}_{\boldsymbol{\sigma\pi}}$ and minimize the LS error along varying weighted directions. In our experiments (see Section 4.2), fixed vectors $\mathbf{w}$ and $\mathbf{v}$ provided accurate approximations and therefore we do not pursue the idea of choosing different vectors here. The interpolatory parametric-Loewner approach [27] handles the vector-valued problems, i.e., $\mathbf{H}(s_i, p_j) \in \mathbb{C}^{n_{out} \times 1}$, in a similar manner by choosing $\mathbf{w}$ as vector of ones (and $\mathbf{v} = 1$ since $n_{in} = 1$). Moreover, recently [20] developed the block-AAA algorithm, which uses a generalized barycentric formula with matrix-valued weights. Further extending that theory to parametric problems could offer different avenues to handle the parametric matrix-valued problems. Extending the framework of [38] to parametric MIMO problems might also provide potential directions. These issues will be investigated in future works.

4.2. Numerical Examples: Stationary PDEs. We consider two examples from [12]. First is the following stationary PDE, briefly mentioned in Section 1:

$$(4.10) \qquad u_{xx} + pu_{yy} + zu = 10\sin(8x(y-1)) \quad \text{on } \Omega = [-1,1] \times [-1,1],$$

with homogeneous Dirichlet boundary conditions. The solution $u(x, y)$ depends on two the parameters (p, z) and is independent of time. Therefore, the model is not a dynamical system, unlike our previous examples, yet this does not matter for our formulation since we simply view the solution as a function of two-variables. The *truth model* is obtained via a spectral Chebyshev collocation approximation with 49 nodes in each direction. We choose to approximate $u(x, y)$ on the whole domain Ω; thus the output is the full solution, leading to a two-variable vector-valued function to sample $\mathbf{H}(p, z) \in \mathbb{R}^{2401 \times 1}$. For our MIMO p-AAA terminology, we interpret this as a model with $n_{in} = 1$ and $n_{out} = 2401$. We take $N = M = 10$ linearly spaced measurements of $\mathbf{H}(p, z)$ in the parameter space $[0.1, 4] \times [0, 2]$. In (4.4), we set $\mathbf{w} = \widetilde{\mathbf{w}}/\|\widetilde{\mathbf{w}}\|_2$ where the entries of $\widetilde{\mathbf{w}} \in \mathbb{R}^{2401}$ result from a standard normal distribution. Also, $\mathbf{v} = 1$ in this example. The usual projection-based approaches to PMoR would form a global basis from these samples and project the truth model into a low-dimensional space. However, we do not assume access to the truth model; but only its samples via black-box simulation, and construct our approximation directly from samples. MIMO p-AAA leads to an approximation with orders $q = 3$ in p and $o = 3$ in z. To judge the quality of the approximation, we perform a parameter sweep in the full parameter domain and find the worst case scenario in terms of the maximum error between the truth model and the MIMO p-AAA approximation over Ω. The worst-case approximation occurs for $p = 1.7545$ and $z = 2$, with an error of 3.11×10^{-2}, showing that the MIMO p-AAA approximant is accurate even in the worst-case. This worst case scenario is depicted in the *left-pane* of Figure 7 where the top-plot shows the truth model, the middle one the MIMO p-AAA approximation, and the bottom one

the error plot. As the figure illustrates, MIMO p-AAA is able to recover the solution on the whole domain accurately.

We also apply MIMO p-AAA to a slightly revised PDE from [12]:

$$(4.11) \qquad (1 + px)u_{xx} + (1 + zy)u_{yy} = e^{4xy} \qquad \text{on } \Omega = [-1, 1] \times [-1, 1].$$

The set-up is the same as above: Dirichlet boundary conditions and the *truth model* obtained via Chebyshev collocation, with 49 nodes in each direction, leading to a two-variable vector-valued function to sample $\mathbf{H}(p, z) \in \mathbb{R}^{2401 \times 1}$. We sample $\mathbf{H}(p, z)$ at $N = M = 10$ linearly spaced points in the parameter domain $(p, z) \in [-0.99, 0.99] \times [-0.99, 0.99]$ and apply MIMO p-AAA. We set $\mathbf{w} = \widetilde{\mathbf{w}}/\|\widetilde{\mathbf{w}}\|_2$ where the entries of $\widetilde{\mathbf{w}}$ result from a uniform random distribution. As stated in [12], this problem is harder to approximate than the first one due to near singularities at the corners of the parameter domain. This is automatically reflected in the approximation orders MIMO p-AAA chooses: $q = 5$ in p and $o = 6$ in z. As for the first PDE, we perform a parameter sweep in the full parameter domain to find the worst-case performance. In this case, the worst approximation occurs for $p = 0.95$ and $z = 0.99$, with an error of 7.28×10^{-2}, an accurate approximation even in the worst case. We show the results from this worst case in the *right-pane* of Figure 7 where the top-plot shows the truth model, the middle one the MIMO p-AAA approximation, and the bottom one the error plot. As in the previous case, MIMO p-AAA accurately captures the full solution.

5. Conclusions. We have presented a data-driven modeling framework for approximating parametric (dynamical) systems by extending the AAA algorithm to multivariate problems. The method does not require access to an internal state-space description and works with function evaluations. We have discussed the scalar-valued problem as well as the matrix-valued ones. Various numerical examples have been used to illustrate the effectiveness of the proposed approach.

REFERENCES

[1] B. D. O. ANDERSON AND A. C. ANTOULAS, *Rational interpolation and state-variable realizations*, Linear Algebra and its Applications, 137–138 (1990), pp. 479–509.
[2] A. C. ANTOULAS AND B. D. O. ANDERSON, *On the scalar rational interpolation problem*, IMA Journal of Mathematical Control and Information, 3 (1986), pp. 61–88.
[3] A. C. ANTOULAS, C. BEATTIE, AND S. GUGERCIN, *Interpolatory methods for model reduction*, Computational Science and Engineering 21, SIAM, Philadelphia, 2020.
[4] A. C. ANTOULAS, A. C. IONITA, AND S. LEFTERIU, *On two-variable rational interpolation*, Linear Algebra and its Applications, 436 (2012), pp. 28890–2915.
[5] A. C. ANTOULAS, S. LEFTERIU, AND A. C. IONITA, *A tutorial introduction to the Loewner framework for model reduction*, in Model Reduction and Approximation, SIAM, 2017, ch. 8, pp. 335–376.
[6] U. BAUR, P. BENNER, C. A. BEATTIE, AND S. GUGERCIN, *Interpolatory projection methods for parameterized model reduction*, SIAM J. Sci. Comput., 33 (2011), pp. 2489–2518.
[7] P. BENNER, A. COHEN, M. OHLBERGER, AND K. WILLCOX, *Model Reduction and Approximation*, SIAM, Philadelphia, PA, 2017.
[8] P. BENNER, S. GUGERCIN, AND K. WILLCOX, *A survey of projection-based model reduction methods for parametric dynamical systems*, SIAM Rev., 57 (2015), pp. 483–531.
[9] P. BENNER AND T. STYKEL, *Model order reduction for differential-algebraic equations: a survey*, in Surveys in Differential-Algebraic Equations IV, Springer, 2017, pp. 107–160.
[10] M. BERLJAFA AND S. GÜTTEL, *The RKFIT algorithm for nonlinear rational approximation*, SIAM J. Sci. Comput., 39 (2017), pp. 2049–2071.
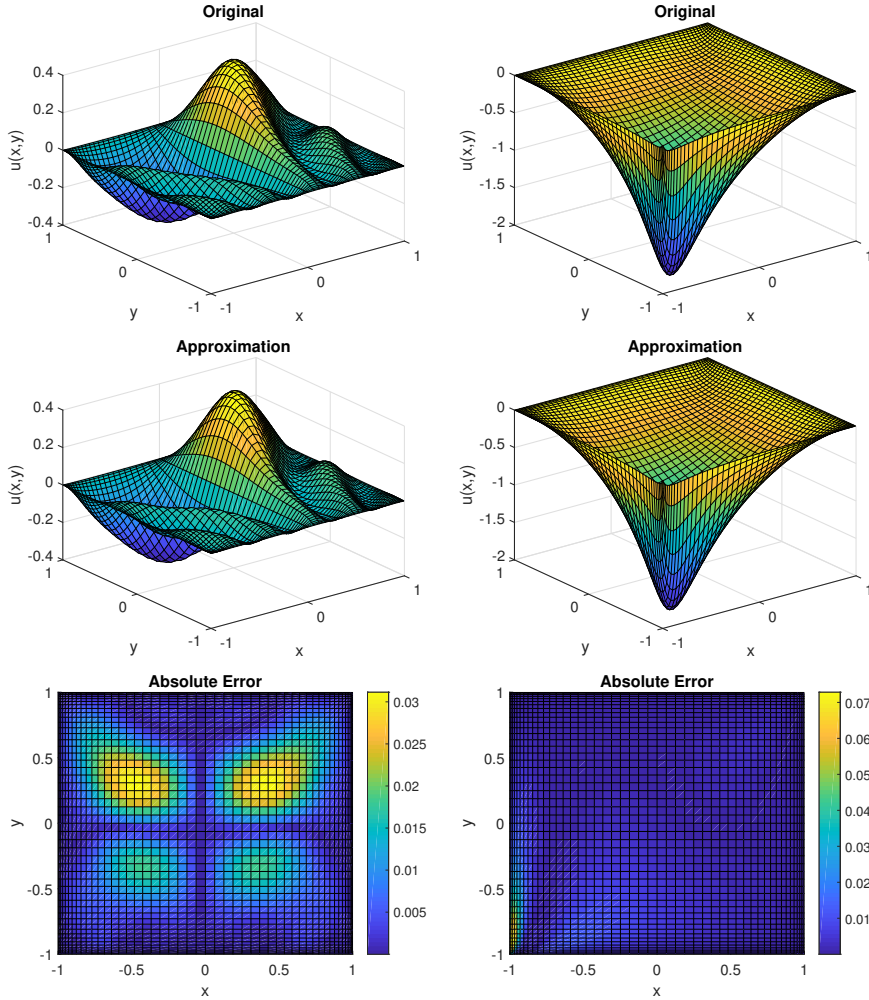
Fig. 7. *Example 4.2.* **MIMO p-AAA** *approximations for two PDEs: left-pane for the PDE in (4.10) for $p = 1.7545$ and $z = 2$ and right-pane for the PDE in (4.11) for $p = 0.95$ and $z = 0.99$)*

[11] J. P. Berrut and L. N. Trefethen, *Barycentric Lagrange interpolation*, SIAM Rev., 46 (2004), pp. 501–517.

[12] Y. Chen, J. Jiang, and A. Narayan, *A robust error estimator and a residual-free error indicator for reduced basis methods*, Computers & Mathematics with Applications, 77 (2019), pp. 1963–1979.

[13] Z. Drmač, S. Gugercin, and C. Beattie, *Vector fitting for matrix-valued rational approximation*, SIAM J. Sci. Comput., 37 (2015), pp. A2346–A2379.

[14] V. Druskin, C. Lieberman, and M. Zaslavsky, *On adaptive choice of shifts in rational Krylov subspace reduction of evolutionary problems*, SIAM J. Sci. Comput., 32 (2010), pp. 2485–2496.

[15] S. Elsworth and S. Güttel, *Conversions between barycentric, RKFUN, and Newton representations of rational interpolants*, Linear Algebra and its Applications, 576 (2019), pp. 246–257.

[16] M. Embree and A. C. Ioniţă, *Pseudospectra of loewner matrix pencils*, in Realization and Model Reduction of Dynamical Systems: A Festschrift in Honor of the 70th Birthday of Thanos Antoulas, C. Beattie, P. Benner, M. Embree, S. Gugercin, and S. Lefteriu, eds., Springer International Publishing, Cham, 2022, pp. 59–78.

[17] L. FENG AND P. BENNER, *A new error estimator for reduced-order modeling of linear parametric systems*, IEEE Transactions on Microwave Theory and Techniques, 67 (2019), pp. 4848–4859.

[18] S. FILIP, Y. NAKATSUKASA, L. N. TREFETHEN, AND B. BECKERMANN, *Rational minimax approximation via adaptive barycentric representations*, SIAM J. Sci. Comput., 40 (2018), pp. A2427–A2455.

[19] P. GONNET, R. PACHÓN, AND L. N. TREFETHEN, *Robust rational interpolation and least-squares*, Electronic Transactions on Numerical Analysis, 38 (2011), pp. 146–167.

[20] I. V. GOSEA AND S. GÜTTEL, *Algorithms for the rational approximation of matrix-valued functions*, SIAM Journal on Scientific Computing, 43 (2021), pp. A3033–A3054.

[21] S. GRIVET-TALOCIA AND B. GUSTAVSEN, *Passive macromodeling: Theory and applications*, vol. 239, John Wiley & Sons, 2015.

[22] S. GUGERCIN, T. STYKEL, AND S. WYATT, *Model reduction of descriptor systems by interpolatory projection methods*, SIAM J. Sci. Comput., 35 (2013), pp. B1010–B1033.

[23] B. GUSTAVSEN AND A. SEMLYEN, *Rational approximation of frequency domain responses by vector fitting*, IEEE Transactions on Power Delivery, 14 (1999), pp. 1052–1061.

[24] J. S. HESTHAVEN, G. ROZZA, AND B. STAMM, *Certified reduced basis methods for parametrized partial differential equations*, Springer Briefs in Mathematics, Springer, Switzerland, 2016.

[25] J. M. HOKANSON, *Projected nonlinear least squares for exponential fitting*, SIAM J. Sci. Comput., 39 (2017), pp. A3107–A3128.

[26] J. M. HOKANSON AND C. C. MAGRUDER, *Least squares rational approximation*, arXiv preprint arXiv:1811.12590, (2018).

[27] A. C. IONITA AND A. C. ANTOULAS, *Data-driven parametrized model reduction in the Loewner framework*, SIAM J. Sci. Comput., 36 (2014), pp. A984–A1007.

[28] D. S. KARACHALIOS, I. V. GOSEA, AND A. C. ANTOULAS, *Data-driven approximation methods applied to non-rational functions*, PAMM, 18 (2018), p. e201800368.

[29] D. S. KARACHALIOS, I. V. GOSEA, Q. ZHANG, AND A. C. ANTOULAS, *Case study: Approximations of the bessel function*, arXiv preprint arXiv:1801.03390, (2017).

[30] C. L. LAWSON, *Contribution to the theory of linear least maximum approximation*, Ph. D. dissertation, Univ. Calif., (1961).

[31] S. LEFTERIU AND A. C. ANTOULAS, *A new approach to modeling multiport systems from frequency-domain data*, IEEE Transactions on Computer-Aided Design of Integrated Circuits and Systems, 29 (2010), pp. 14–27.

[32] S. LEFTERIU AND A. C. ANTOULAS, *On the convergence of the vector-fitting algorithm*, IEEE Transactions on Microwave Theory and Techniques, 61 (2013), pp. 1435–1443.

[33] E. LEVY, *Complex curve fitting*, IRE Transactions on Automatic Control, AC-4 (1959), pp. 37–43.

[34] P. LIETAERT, K. MEERBERGEN, J. PÉREZ, AND B. VANDEREYCKEN, *Automatic rational approximation and linearization of nonlinear eigenvalue problems*, IMA Journal of Numerical Analysis, 42 (2022), pp. 1087–1115.

[35] A. J. MAYO AND A. C. ANTOULAS, *A framework for the solution of the generalized realization problem*, Linear Algebra and Its Applications, 425 (2007), pp. 634–662.

[36] V. MEHRMANN AND T. STYKEL, *Balanced truncation model reduction for large-scale systems in descriptor form*, in Dimension Reduction of Large-Scale Systems, Springer, Berlin, 2005, pp. 83–115.

[37] P. MLINARIĆ AND S. GUGERCIN, $\mathcal{L}_2$-*optimal reduced-order modeling using parameter-separable forms*, arXiv preprint arXiv:2206.02929, (2022).

[38] L. MONZÓN, W. JOHNS, S. IYENGAR, M. REYNOLDS, J. MAACK, AND K. PRABAKAR, *A multifunction aaa algorithm applied to frequency dependent line modeling*, in 2020 IEEE Power & Energy Society General Meeting (PESGM), IEEE, 2020, pp. 1–5.

[39] C. MOOSMANN, *ParaMOR - Model Order Reduction for parameterized MEMS applications*, PhD thesis, Albert-Ludwigs-Universität Freiburg, 2007.

[40] Y. NAKATSUKASA, O. SÈTE, AND L. N. TREFETHEN, *The AAA algorithm for rational approximation*, SIAM J. Sci. Comput., 40 (2018), pp. A1494–A1522.

[41] Y. NAKATSUKASA AND L. N. TREFETHEN, *An algorithm for real and complex rational minimax approximation*, SIAM Journal on Scientific Computing, 42 (2020), pp. A3157–A3179.

[42] A. QUARTERONI, A. MANZONI, AND F. NEGRI, *Reduced basis methods for partial differential equations: an introduction*, UNITEXT, Springer Cham, 2016.

[43] C. SANATHANAN AND J. KOERNER, *Transfer function synthesis as a ratio of two complex polynomials*, IEEE Transactions on Automatic Control, 8 (1963), pp. 56–58.

[44] THE MORWIKI COMMUNITY, *Modified gyroscope*. MORwiki – Model Order Reduction Wiki, 2018, http://modelreduction.org/index.php/Modified_Gyroscope.

Appendix A. State-space realization. First, we recall the formulae derived in [27], which allow for computing state-space realizations based on a given two-variable barycentric form. In the following, assume that the barycentric form (3.2) computed by the p-AAA algorithm is given. Define the parameter dependent terms

$$\hat{\alpha}_i(p) = \sum_{j=1}^{q+1} \frac{\alpha_{ij}}{p - \pi_j} \quad \text{and} \quad \hat{\beta}_i(p) = \sum_{j=1}^{q+1} \frac{\beta_{ij}}{p - \pi_j},$$

as well as the system matrices

$$s\hat{\mathbf{E}} - \hat{\mathbf{A}}(p) = \begin{bmatrix} s - \sigma_1 & \sigma_2 - s & & \\ \vdots & & \ddots & \\ s - \sigma_1 & & & \sigma_k - s \\ \hat{\alpha}_1(p) & \hat{\alpha}_2(p) & \dots & \hat{\alpha}_k(p) \end{bmatrix}, \hat{\mathbf{b}} = \begin{bmatrix} 0 \\ \vdots \\ 0 \\ 1 \end{bmatrix}, \hat{\mathbf{c}}(p) = \begin{bmatrix} \hat{\beta}_1(p) \\ \hat{\beta}_2(p) \\ \vdots \\ \hat{\beta}_k(p) \end{bmatrix}.$$

An equivalent representation to the barycentric form (3.2) is then given by

$$\widetilde{H}(s,p) = \hat{\mathbf{c}}(p)^\top (s\hat{\mathbf{E}} - \hat{\mathbf{A}}(p))^{-1}\hat{\mathbf{b}}.$$

For a detailed discussion regrading the connection between the matrix pencil $s\hat{\mathbf{E}} - \hat{\mathbf{A}}(p)$ and the barycentric form we refer the reader to [27]. Note, that the presented matrices, their dimensions and the type of parameter dependence are not unique. For example, an equivalent realization without parameter dependence in $\hat{\mathbf{c}}(p)$ but larger matrices was derived in [4].

Real system matrices. Whenever complex-valued frequencies are used for generating transfer function samples, the matrix $\hat{\mathbf{A}}(p)$ as well as $\hat{\mathbf{c}}(p)$ are also complex-valued. In [27] the authors demonstrate that under the condition that interpolated complex frequencies exclusively appear as complex conjugate pairs, real-valued system matrices can be computed. Note that $H(\overline{s}, p) = \overline{H(s,p)}$ since the underlying system is assumed to be real. This reveals that we can obtain samples from conjugates of complex frequencies without having to compute or measure additional values. Consider the partitioning (3.3) and relabel the frequencies according to the previously mentioned condition:

$$(A.1) \quad \{s_1, \dots, s_N\} = \{\sigma_1, \dots, \sigma_r, \sigma_{r+1}, \overline{\sigma}_{r+1}, \dots, \sigma_{r+c}, \overline{\sigma}_{r+c}\} \cup \{\hat{\sigma}_1, \dots, \hat{\sigma}_{N-k}\},$$

where $\sigma_1, \dots, \sigma_r$ are real-valued, $\sigma_{r+1}, \dots, \sigma_{r+c}$ are complex-valued and $k = r + 2c$. First, as done in [27], consider the case $r \geq 1$ in (A.1) and define the matrices

$$\mathbf{J} = \frac{1}{\sqrt{2}} \begin{bmatrix} 1 & 1 \\ -i & i \end{bmatrix}, \mathbf{U} = \begin{bmatrix} \mathbf{I}_{r-1} & & \\ & \mathbf{I}_c \otimes \mathbf{J} & \\ & & 1 \end{bmatrix}, \mathbf{V} = \begin{bmatrix} \mathbf{I}_r & \\ & \mathbf{I}_c \otimes \mathbf{J} \end{bmatrix}.$$

A realization consisting only of real matrices is then given by $\hat{\mathbf{b}}_r = \mathbf{U}\hat{\mathbf{b}} = \hat{\mathbf{b}}$, $\hat{\mathbf{c}}_r = \hat{\mathbf{c}}\mathbf{V}^*$ and $s\hat{\mathbf{E}}_r - \hat{\mathbf{A}}_r(p) = s\mathbf{U}\hat{\mathbf{E}}\mathbf{V}^* - \mathbf{U}\hat{\mathbf{A}}(p)\mathbf{V}^*$, such that

$$\widetilde{H}(s,p) = \hat{\mathbf{c}}_r(p)^\top (s\hat{\mathbf{E}}_r - \hat{\mathbf{A}}_r(p))^{-1}\hat{\mathbf{b}}_r.$$

Following [27], one can write the real system matrices explicitly as

$$\hat{\mathbf{c}}_r^\top = \begin{bmatrix} \hat{\beta}_1(p), \dots, \hat{\beta}_r(p), \text{Re}(\hat{\beta}_{r+1}(p)), -\text{Im}(\hat{\beta}_{r+1}(p)), \dots, \text{Re}(\hat{\beta}_{r+c}(p)), -\text{Im}(\hat{\beta}_{r+c}(p)) \end{bmatrix}$$

and

$$
s\hat{\mathbf{E}}_r - \hat{\mathbf{A}}_r(p) = \begin{bmatrix} s-\sigma_1 & \sigma_2 - s & & & & & \\ \vdots & & \ddots & & & & \\ s-\sigma_1 & & & \sigma_r - s & & & \\ \mathbf{f} & & & & \mathbf{g}_{r+1} & & \\ \vdots & & & & & \ddots & \\ \mathbf{f} & & & & & & \mathbf{g}_{r+c} \\ \hat{\alpha}_1(p) & \hat{\alpha}_2(p) & \cdots & \hat{\alpha}_r(p) & \gamma_{r+1}(p) & \cdots & \gamma_{r+c}(p) \end{bmatrix},
$$

where $\mathbf{f} = \begin{bmatrix} s - \sigma_1 \\ 0 \end{bmatrix}$, $\mathbf{g}_i = \begin{bmatrix} \operatorname{Re}\sigma_i - s & -\operatorname{Im}\sigma_i \\ \operatorname{Im}\sigma_i & \operatorname{Re}\sigma_i - s \end{bmatrix}$ and $\gamma_i^\top = \begin{bmatrix} \operatorname{Re}\hat{\alpha}_i(p) \\ -\operatorname{Im}\hat{\alpha}_i(p) \end{bmatrix}$.

In our dynamical system examples, we have $r = 0$ in (A.1), i.e., we do not have a real frequency sample. We now provide some modifications to handle this case. For $r = 0$, we define the vector $\ell = \frac{1}{\sqrt{2}} \begin{bmatrix} 1 & \cdots & 1 \end{bmatrix} \otimes \begin{bmatrix} -1 & 0 \end{bmatrix}$ and

$$
\mathbf{U}_0 = \begin{bmatrix} \frac{i}{\sqrt{2}} & & \\ \ell^\top & \mathbf{I}_{c-1} \otimes \mathbf{J} & \\ & & 1 \end{bmatrix}.
$$

We then obtain

$$
s\hat{\mathbf{E}}_c - \hat{\mathbf{A}}_c(p) = s\mathbf{U}_0\hat{\mathbf{E}}\mathbf{V}^* - \mathbf{U}_0\hat{\mathbf{A}}(p)\mathbf{V}^* = \begin{bmatrix} \tilde{\mathbf{f}}_0 & & & \\ \tilde{\mathbf{f}} & \mathbf{g}_2 & & \\ \vdots & & \ddots & \\ \tilde{\mathbf{f}} & & & \mathbf{g}_c \\ \gamma_1(p) & \gamma_2(p) & \cdots & \gamma_c(p) \end{bmatrix},
$$

where $\tilde{\mathbf{f}}_0^\top = \begin{bmatrix} \operatorname{Im}(\sigma_1) \\ \operatorname{Re}(\sigma_1) - s \end{bmatrix}$ and $\tilde{\mathbf{f}} = \begin{bmatrix} s - \operatorname{Re}(\sigma_1) & \operatorname{Im}(\sigma_1) \\ 0 & 0 \end{bmatrix}$. Using $\hat{\mathbf{c}}_r(p)$ and $\hat{\mathbf{b}}_r$ from the previously discussed case we obtain the real state-space form

$$
\widetilde{H}(s,p) = \hat{\mathbf{c}}_r(p)^\top (s\hat{\mathbf{E}}_c - \hat{\mathbf{A}}_c(p))^{-1}\hat{\mathbf{b}}_r.
$$

Appendix B. Minimal order interpolant. A key result in [27] reveals that the minimal order of a two-variable rational interpolant is given by (k_*, q_*), where

(B.1) $$ k_* = \max_{j=1,\dots,M} \operatorname{rank} \mathbb{L}_{p_j} \quad \text{and} \quad q_* = \max_{i=1,\dots,N} \operatorname{rank} \mathbb{L}_{s_i}, $$

and the 1D Loewner matrices $\mathbb{L}_{p_j}$ and $\mathbb{L}_{s_i}$ are defined in (3.12) and (3.8), respectively. Moreover, any partitioning as in (3.3) with $k > k_*$ and $q > q_*$ yields a rational function that interpolates all function samples. In other words, one could compute a priori upper bounds for the order of the approximant by computing $M + N$ SVDs of 1D Loewner matrices and avoid constructing non-minimal interpolants when using the p-AAA algorithm. Note that for large data sets this is a potentially expensive task. Instead, we propose an approach, which computes a minimal interpolant via a post-processing procedure. First, we answer the question of how we can tell whether the output from Algorithm 3.1 is a non-minimal interpolant or not without computing k_* and q_* as in (B.1).

LEMMA B.1. *Consider the data* (3.3) *and let the corresponding barycentric rational approximant* $\widetilde{H}(s, p)$ *have the form in* (3.2). *Furthermore, for at least one* $\tilde{p} \in \{p_j\}$ *and* $\tilde{s} \in \{s_i\}$ *satisfying* $k_* = \operatorname{rank} \mathbb{L}_{\tilde{p}}$ *and* $q_* = \operatorname{rank} \mathbb{L}_{\tilde{s}}$, *we assume that all* $k_* \times k_*$ *submatrices of* $\mathbb{L}_{\tilde{p}}$ *and* $q_* \times q_*$ *submatrices of* $\mathbb{L}_{\tilde{s}}$ *have full rank. Then*

$$\dim \ker \mathbb{L}_2 \geq 1 \quad \textit{if and only if} \quad k > k_* \textit{ and } q > q_*.$$

In addition, if $\dim \ker \mathbb{L}_2 \geq 1$, *then* $\dim \ker \mathbb{L}_2 = (k - k_*)(q - q_*)$.

Proof. We will only show the first implication ($\Rightarrow$) and refer the reader to [27] for the proof of the other direction ($\Leftarrow$). Let $\dim \ker \mathbb{L}_2 \geq 1$ and assume that $k \leq k_*$ or $q \leq q_*$. First, $\dim \ker \mathbb{L}_2 \geq 1$ implies that $\widetilde{H}(s, p)$ interpolates all data in (3.3) (this follows from the error formula derived in Corollary 4.3 in [27]). Let $\tilde{p}$ be a parameter where the first expression in (B.1) attains its maximum. In other words $k_* = \operatorname{rank} \mathbb{L}_{\tilde{p}}$. Further, assume that all $k_* \times k_*$ submatrices of $\mathbb{L}_{\tilde{p}}$ have full rank. These conditions imply that a rational interpolant of the values $H(s_i, \tilde{p})$ for $i = 1, \dots, N$ has to be at least of order k_* [3]. However, $\widetilde{H}(s, \tilde{p})$ interpolates all these points and is of order $k_* - 1$ or less. A similar contradiction can be shown in the case that $q \leq q_*$ yielding that $k > k_*$ and $q > q_*$. Based on this result, we can apply Theorem 4.2. from [27] which implies that $\operatorname{rank} \mathbb{L}_2 = kq - (k - k_*)(q - q_*)$. Since $\mathbb{L}_2$ has kq columns we obtain $\dim \ker \mathbb{L}_2 = (k - k_*)(q - q_*)$. □

Algorithmic implications. Lemma B.1 reveals a connection between the nullity of $\mathbb{L}_2$ and the minimal order of an interpolant, based on uniform rank conditions of 1D Loewner matrices that are typically satisfied in practice [3]. If $\dim \ker \mathbb{L}_2 = d = 1$ we have $k = k_* + 1$ and $q = q_* + 1$ and the interpolant is of minimal order. If $d > 1$ it must be that $k > k_* + 1$ or $q > q_* + 1$ and the interpolant is of non-minimal order. Assuming that we compute the SVD of $\mathbb{L}_2$ using direct methods, d is available in each step of the algorithm without the need for additional computations. Our proposed post-processing procedure, which can be used after Line 16 of Algorithm 3.1 if $d > 1$, is as follows:

1. If $q \leq k$ compute q_* based on (B.1) and if $k < q$ compute k_* based on (B.1).
2. Lemma B.1 implies that $k_* = k - d/(q - q_*)$ and $q_* = q - d/(k - k_*)$. From the first step we either obtain k_* or q_*. In the former case we compute $q_* = q - d/(k - k_*)$ whereas in the latter case we compute $k_* = k - d/(q - q_*)$ in order to obtain the order of the minimal interpolant (k_*, q_*).
3. Update the partitioning (3.3) such that $k = k_* + 1$ and $q = q_* + 1$ and use it to compute $\widetilde{H}$ based on Lines 16 and 17 of Algorithm 3.1.